On the Bone Tissue Response to Surface Chemistry Modifications of Titanium Implants

by

Byung-Soo Kang

UNIVERSITY OF GOTHENBURG

Department of Biomaterials, Institute of Clinical Sciences
Sahlgrenska Academy at University of Gothenburg
Gothenburg, Sweden

2011

Department of Biomaterials
Institute of Clinical Sciences
Sahlgrenska Academy
University of Gothenburg

Correspondence:
Byung-Soo Kang
Department of Biomaterials
Institute of Clinical Sciences
Sahlgrenska Academy at University of Gothenburg
Box 412
Arvid WallgrensBacke 20
SE 413 46 Gothenburg
Sweden

E-mail: byung-soo.kang@biomaterials.gu.se

ISBN: 978-91-628-8325-6
E-publication: http://hdl.handle.net/2077/26273

Printed in Sweden
Geson Hylte Tryck

Printed in 200 copies

To My Parents with Endless Love

This thesis represents number 42 in series of investigations on implants, hard tissue and the locomotor apparatus originating from the department of Biomaterials/Handicap Research, Institute of Clinical Sciences at Sahlgrenska Academy, University of Gothenburg and the department of Prosthodontics, Malmö University, Sweden.

1. **Anders R Eriksson** DDS, 1984. Heat-induced Bone Tissue Injury. An in vivo investigation of heat tolerance of bone tissue and temperature rise in the drilling of cortical bone. Thesis defended 21.2.1984. External examiner: Docent K-G. Thorngren.

2. **Magnus Jacobsson** MD, 1985. On Bone Behaviour after Irradiation. Thesis defended 29.4.1985. External examiner: Docent A. Nathanson.

3. **Fredrik Buch** MD, 1985. On Electrical Stimulation of Bone Tissue. Thesis defended 28.5.1985. External examiner: Docent T. Ejsing-Jörgensen.

4. **Peter Kälebo** MD, 1987. On Experimental Bone Regeneration in Titanium Implants. A quantitative microradiographic and histologic investigation using the Bone Harvest Chamber. Thesis defended 1.10.1987. External examiner: Docent N. Egund.

5. **Lars Carlsson** MD, 1989. On the Development of a new Concept for Orthopaedic Implant Fixation. Thesis defended 2.12.1989. External examiner: Docent L-Å Broström.

6. **Tord Röstlund** MD, 1990. On the Development of a New Arthroplasty. Thesis defended 19.1.1990. External examiner: Docent Å. Carlsson.

7. **Carina Johansson** Techn Res, 1991. On Tissue Reactions to Metal Implants. Thesis defended 12.4.1991. External examiner: Professor K. Nilner.

8. **Lars Sennerby** DDS, 1991. On the Bone Tissue Response to Titanium Implants. Thesis defended 24.9.1991. External examiner: Dr J.E. Davis.

9. **Per Morberg** MD, 1991. On Bone Tissue Reactions to Acrylic Cement. Thesis defended 19.12.1991. External examiner: Docent K. Obrant.

10. **Ulla Myhr** PT, 1994. On Factors of Importance for Sitting in Children with Cerebral Palsy. Thesis defended 15.4.1994. External examiner: Docent K. Harms-Ringdahl.

11. **Magnus Gottlander** MD, 1994. On Hard Tissue Reactions to Hydroxyapatite-Coated Titanium Implants. Thesis defended 25.11.1994. External examiner: Docent P. Aspenberg.

12. **Edward Ebramzadeh** MScEng, 1995. On Factors Affecting Long-Term Outcome of Total Hip Replacements. Thesis defended 6.2.1995. External examiner: Docent L. Linder.

13. **Patricia Campbell** BA, 1995. On Aseptic Loosening in Total Hip Replacement: the Role of UHMWPE Wear Particles. Thesis defended 7.2.1995. External examiner: Professor D. Howie.

14. **Ann Wennerberg** DDS, 1996. On Surface Roughness and Implant Incorporation. Thesis defended 19.4.1996. External examiner: Professor P.-O. Glantz.

15. **Neil Meredith** BDS MSc FDS RCS, 1997. On the Clinical Measurement of Implant Stability and Osseointegration. Thesis defended 3.6.1997. External examiner: Professor J. Brunski.

16. **Lars Rasmusson** DDS, 1998. On Implant Integration in Membrane-Induced and Grafter Bone. Thesis defended 4.12.1998. External examiner: Professor R. Haanaes.

17. **Thay Q Lee** MSc, 1999. On the Biomechanics of the Patellofemoral Joint and Patellar Resurfacing in Total Knee Arthroplasty. Thesis defended 19.4.1999. External examiner: Docent G. Nemeth.

18. **Anna Karin Lundgren** DDS, 1999. On Factors Influencing Guided Regeneration and Augmentation of Intramembraneous Bone. Thesis defended 7.5.1999. External examiner: Professor B. Klinge.

19. **Carl-Johan Ivanoff** DDS, 1999. On Surgical and Implant Related Factors Influencing Integration and Function of Titanium Implants. Experimental and Clinical Aspects. Thesis defended 12.5.1999. External examiner: Professor B. Rosenquist.

20. **Bertil Friberg** DDS MDS, 1999. On Bone Quality and Implant Stability Measurements. Thesis defended 12.11.1999. External examiner: Docent P. Åstrand.

21. **Åse Allansdotter Johnsson** MD, 1999. On Implant Integration in Irradiated Bone. An Experimental Study of the Effects of Hyberbaric Oxygenation and Delayed Implant Placement. Thesis defended 8.12.1999. External examiner: Docent K. Arvidsson-Fyrberg.

22. **Börje Svensson** DDS, 2000. On Costochondral Grafts Replacing Mandibular Condyles in Juvenile Chronic Arthritis. A Clinical, Histologic and Experimental Study. Thesis defended 22.5.2000. External examiner: Professor Ch. Lindqvist.

23. **Warren Macdonald** BEng, MPhil, 2000. On Component Integration in Total Hip Arthroplasty: Pre-Clinical Evaluations. Thesis defended 1.9.2000. External examiner: Dr A.J.C. Lee.

24. **Magne Røkkum** MD, 2001. On Late Complications with HA Coated Hip Asthroplasties. Thesis defended 12.10.2001. External examiner: Professor P. Benum.

25. **Carin Hallgren Höstner** DDS, 2001. On the Bone Response to Different Implant Textures. A 3D analysis of roughness, wavelength and surface pattern of experimental implants. Thesis defended 9.11.2001. External examiner: Professor S. Lundgren.

26. **Young-Taeg Sul** DDS, 2002. On the Bone Response to Oxidised Titanium Implants: The role of microporous structure and chemical composition of the surface oxide in enhanced osseointegration. Thesis defended 7.6.2002. External examiner: Professor J.-E. Ellingsen.

27. **Victoria Franke Stenport** DDS, 2002. On Growth Factors and Titanium Implant Integration in Bone. Thesis defended 11.6.2002. External examiner: Associate Professor E. Solheim.

28. **Mikael Sundfeldt** MD, 2002. On the Aetiology of Aseptic Loosening in Joint Arthroplasties and Routes to Improved cemented Fixation. Thesis defended 14.6.2002. External examiner: Professor N Dahlén.

29. **Christer Slotte** DDS, 2003. On Surgical Techniques to Increase Bone Density and Volume. Studies in the Rat and the Rabbit. Thesis defended 13.6.2003. External examiner: Professor C.H.F. Hämmerle.

30. **Anna Arvidsson** MSc, 2003. On Surface Mediated Interactions Related to Chemo-mechanical Caries Removal. Effects on surrounding tissues and materials. Thesis defended 28.11.2003. External examiner: Professor P. Tengvall.

31. **Pia Bolind** DDS, 2004. On 606 Retrieved Oral and Cranio-facial Implants. An analysis of consecutively received human specimens. Thesis defended 17.12. 2004. External examiner: Professor A. Piattelli.

32. **Patricia Miranda Burgos** DDS, 2006. On the Influence of Micro-and Macroscopic Surface Modifications on Bone Integration of Titanium Implants. Thesis defended 1.9. 2006. External examiner: Professor A. Piattelli.

33. **Jonas P Becktor** DDS, 2006. On Factors Influencing the Outcome of Various Techniques Using Endosseous Implants for Reconstruction of the Atrophic Edentulous and Partially Dentate Maxilla. Thesis defended 17.11.2006. External examiner: Professor K. F. Moos

34. **Anna Göransson** DDS, 2006. On Possibly Bioactive CP Titanium Surfaces. Thesis defended 8.12.2006 External examiner: B. Melsen

35. **Andreas Thor** DDS, 2006. On Platelet-rich Plasma in Reconstructive Dental Implant Surgery. Thesis defended 8.12.2006. External examiner: Professor E.M. Pinholt.

36. **Luiz Meirelles** DDS MSc, 2007. On Nano Size Structures For Enhanced Early Bone Formation. Thesis defended 13.6.2007. External examiner: Professor Lyndon F. Cooper.

37. **Pär-Olov Östman** DDS, 2007. On Various Protocols for Direct Loading of Implant-supported Fixed Prostheses. Thesis defended 21.12.2007. External examiner: Professor B Klinge

38. **Kerstin Fischer** DDS, 2008. On Immediate/Early Loading of Implant Supported Prostheses in the Maxilla. Thesis defended 8.2.2008. External examiner: Professor Kristina Arvidson Fyrberg

39. **Alf Eliasson** 2008. On the Role of Number of Fixtures, Surgical Technique and Timing of Loading. Thesis defended 23.5.2008. External examiner: Kristina Arvidson-Fyrberg.

40. **Victoria Fröjd** DDS, 2010. On Ca^{2+} Incorporation and Nanoporosity of Titanium Surfaces and the Effect on Implant Performance. Thesis defended 26.11.2010. External examiner: Professor J. E. Ellingsen.

41. **Lory Melin Svanborg** DDS, 2011. On the Importance of Nanometer Structures for Implant Incorporation in Bone Tissue. Thesis defended 01.06.2011. External examiner: Associate professor Christer Dahlin

42**. Byung-Soo Kang** MSc, 2011. On the Bone Tissue Response to Surface Chemistry Modifications of Titanium Implants. Thesis to be defended 30.09.2011. External examiner: Professor Jinshan Pan.

Abstract

Background: Surface properties of titanium implants play an important role in osseointegration. From 1990, a lot of engineering techniques have been applied to dental implant productions for improving their clinical performance by changing surface properties. In particular, surface chemistry modification enhanced the strength and speed of implant integration in bone and has become a marketing trend in the production of new implants. However, it is not clearly understood why and how strongly surface chemistry modifications reinforce the osseointegration of titanium. Hence, it is required to investigate the bone response to surface chemistry modifications of titanium for a better understanding of the roles of surface chemistry on the osseointegration response.

Aims: The present thesis aims to investigate the bone response to chemistry-modified titanium implants. In particular, our purpose is to better understand the effect of surface chemistry on the osseointegration of titanium implants.

Materials and methods: Clinical implants, such as TiUnite, Osseotite, OsseoSpeed and SLA were analyzed. Surface engineering methods include plasma immersion ion implantation and deposition (PIIID) and micro arc oxidation (MAO). Using these techniques, Mg-, Ca- and O-incorporated titanium surfaces were prepared. Surface chemistry was analyzed by X-ray photoelectron spectroscopy and auger electron spectroscopy. For topographical analyses, we used scanning electron microscopy and optical interferometry. A total of 136 screw-shape implants were inserted into rabbit tibiae and the bone responses were evaluated after 3, 6 and 10 weeks of healing. Biomechanical strengths at the bone implant interface were measured by removal torque. Bone tissue responses were evaluated by quantifying bone metal contact, bone area and new bone formation from undecalcified cut and ground sections.

Results: Surface chemistry of the Osseotite, OsseoSpeed and SLA implants showed mainly TiO_2, but surface topography varied with modification methods in use. In contrast, the TiUnite, prepared by an electrochemical oxidation technique, displayed porous structures as well as P-incorporation to the oxide layer. The PIIID process changed surface chemistry of titanium with plasma resources, but negligibly altered surface topography at the nanometer scale. The atom concentration of plasma ion increased with ion dose, but decreased with acceleration voltage. The MAO process not only incorporated Mg and Ca ions into titanium surfaces, but also produced microporous structures on the surface. Furthermore, the MAO process controlled the calcium concentration of titanium implants without significant change of chemical bonding states of Ca in titanium oxide. *In vivo* results showed that Mg-incorporated implants produced by the MAO technique increased the biomechanical bonding strength and osseointegration rate compared to non-incorporated titanium surfaces. Furthermore, Mg-incorporated implants produced by the PIIID demonstrated a significant increase of biomechanical bonding strength, bony contact and new bone formation compared to O-incorporated implants. Ca 4.2% and Ca 6.6% containing implants revealed no significant differences in biomechanical and histomorphometrical measurement outcomes in rabbit tibiae.

Conclusions: The surface chemistry and topography of clinical and experimental implants were greatly dependent of surface engineering methods. In particular, the PIIID technique modified surface chemistry of titanium implants by tailoring plasma source with negligible alternation of surface topography at the nanometer scale, thus enabling the investigation of the effect of bioactive implant surface chemistry on the bone response. Using the PIIID and MAO techniques, we found that the Mg-incorporation to titanium significantly enhanced the bone responses to implant surfaces. Furthermore, the Mg-incorporated titanium oxide chemistry played an important role on the strength and speed of osseointegration. Choosing one of two calcium concentrations had no significant influence on the bone response to the Ca-incorporated titanium implants.

Key words: Osseointegrated titanium implants, magnesium and calcium incorporated bioactive titanium oxide, metal plasma immersion ion implantation and deposition, micro arc oxidation, clinical implants, *in vivo* bone response

List of Papers

This thesis is based on the following original articles and manuscript:

Study I. Byung-Soo Kang, Young-Taeg Sul, Se-Jung Oh, Hyun-Ju Lee, Tomas Albrektsson.
XPS, AES and SEM analysis of recent dental implants.
Acta Biomater, 2009 Jul; 5 (6): 2222-29

Study II. Byung-Soo Kang, Young-Taeg Sul, Yongsoo Jeong, Eungsun Byon, Jong-Kuk Kim, Suyeon Cho, Se-Jung Oh, Tomas Albrektsson
Metal plasma immersion ion implantation and deposition (MePIIID) on screw-shaped titanium implant: The effects of ion source, ion dose and acceleration voltage on surface chemistry and morphology
Med Eng Phys, 2011Jul;33(6):730-38

Study III. Young-Taeg Sul, Byung-Soo Kang, Carina Johansson, Heung-Sik Um, Chan-Jin Park, Tomas Albrektsson.
The roles of surface chemistry and topography in the strength and rate of osseointegration of titanium implants in bone
J Biomed Mater Res A, 2009 Jun 15;89(4):942-50

Study IV. Byung-Soo Kang, Young-Taeg Sul, Carina Johansson, Se-Jung Oh, Hyun-Ju Lee, Tomas Albrektsson
The effect of calcium ion concentration on the bone response to oxidized titanium implants
Clin Oral Implants Res, 2011 [Epub ahead of print]

Study V. Byung-Soo Kang, Young-Taeg Sul, Carina Johansson , Hyung-Seop Kim, Tomas Albrektsson
Bone response to plasma immersion ion implantation and deposition of titanium implants with oxygen and magnesium
In Manuscript

Table of Contents

Nomenclature and Abbreviations

AES	Auger Electron Spectroscopy
Al	Aluminum
AR	As-received
Ar	Argon
At%	Atom Concentration Ratio (%)
BA	Bone Area
BE	Binding Energy (eV)
BMC	Bone Metal Contact
C	Carbon
CNC	Computer Numerical Control
Cp titanium	Commercially Pure Titanium
Ca	Calcium
eV	Electron Volt, 1eV = 1.6×10^{-19} Joule
F	Fluorine
H	Hydrogen
HA	Hydroxyapatite
MAO	Micro Arc Oxidation
MePIIID	Metal Plasma Immersion Ion Implantation and Deposition
Mg	Magnesium
MPa	Mega Pascals, 1MPa = 10^6 N/m^2
N	Nitrogen
Na	Sodium
NB	New Bone
K	Potassium
O	Oxygen
OC	Old Cortical Bone
P	Phosphorous
Pa	Pascal = 1 N/m^2
PIIID	Plasma Immersion Ion Implantation and Deposition
RB	Red Blood Cell
RTQ	Removal Torque
S	Sulfur
Sa	Arithmetic Average Height Deviation
Sdr	Developed Surface Ratio
SEM	Scanning Electron Microscopy
Si	Silicon
SP	Sputter-cleaned
ST	Soft Tissue
Ti	Titanium
XPS	X-ray Photoelectron Spectroscopy

1 Introduction

1.1 Current Trends of Dental Implants Production

Since titanium implants were first introduced by professor P-I Branemark in 1965 as a viable option for patient treatment[1], a variety of surface properties of osseointegrated implants have been developed to improve clinical performance of titanium implants.[2-13] Unlike the last three decades that was dominated by micro-structured, moderately rough surfaces[3,13,14], today, recent advances of surface engineering micro- and nano-technology provide greater opportunities for high quality surfaces of titanium implants. Thus, newly launched clinical implants have demonstrated the developed surface properties, including bioactive surface chemistry, topography and crystal structures from micro to nanometer scales[11,12,15-17.]

Surface chemistry modification of titanium implants has become a marketing trend in the production of new implants for a better clinical performance. So-called bioactive implants, such as magnesium, calcium, phosphorous and fluorine containing titanium implants have shown promising *in vivo* results with respect to their strength and speed of osseointegration.[9,12,15,18,19] These implants are now available in the market and expected to improve clinical results especially in situations of immediate/early loading or in poor bone quantity and quality situations.

1.2 Needs for Developing Implant Surface Properties and the Effects of Surface Chemistry Modification of Titanium on the Osseointegration

The outermost layer of titanium implants is covered with 2-20 nm thickness of native oxide film[20,21], which forms immediately after exposure to oxygen. The native oxide film increases the corrosion resistance of bulk titanium and provides the biocompatibility of titanium implants in clinical and experimental applications. The clinical success rate of titanium implants has been reported as more than 90% in literature due to stable osseointegration[1,22], which is defined as “a direct – on the light microscopic level– contact between living bone and implant”.[23] Despite good osseointegration of pure titanium oxide, relatively low success rates of osseointegrated implants were reported in poor bone quantity and quality situations.[22,24-26] Furthermore, most of the failures of dental implants in clinical use occurred during the early healing period.[27] For these reasons, we need to develop novel implant surfaces which lead to rapid and strong osseointegration. Surface modification of titanium implants is one of methods to enhance osseointegration in terms of bonding strength and speed of anchorage.[2,12,14,15,18,28] In particular, surface chemistry-modified implants have shown promising results in *in vivo*

experiments. So called "bioactive" implants containing calcium, magnesium, phosphorous, fluorine, sodium, calcium phosphates and hydroxyapatite increased the bonding strength and anchorage speed of implants in bone (see the section 1.6 for detailed information).[7,15,18,28-30] It is not clearly understood yet why the bioactive titanium implants enhanced the osseointegration at the early healing times, but several explanations have been suggested as follows:

i) Chemistry mediated-osseointegration mechanism (Biochemical bonding): Sul et al have found that Ca- and Mg-incorporated titanium implants significantly increased the strength and speed of osseointegration compared to non-incorporated cp titanium.[9,11,12,31,32] On the basis of these findings, Sul et al explained enhanced bone responses to the bioactive implants at the early healing period being facilitated by the biochemical bonding between the implant and bone tissue. According to the bonding mechanism, the Ca and Mg cations in titanium oxide provide numerous binding sites for the attachments of adhesive bone matrix proteins. Thus, Mg- and Ca-incorporated titanium surfaces may electrostatically bond with polyanionic proteins, such as proteoglycans, collagen, thrombospondin, firbronectin, vitronectin, fibrillin, osteoadherin, osteopontin and bone sialoprotein.[33-35] This process can stimulate the Arg-Gly-Asp (RGD) sequence and trigger further recruitment of osteoprogenitor cells and osteoblasts, which possibly leads to rapid and strong bone formation at Mg- and Ca-incorporated titanium.

ii) Electronic charge effects of bioactive implants on the bone formation: Hanawa et al have found an enhanced bone response to Ca-incorporated titanium compared to non-incorporated cp titanium.[18] According to the authors, the rapid healing process of the Ca-incorporated titanium in rat tibiae is most likely due to the positively charged Ca-incorporated titanium by dissociation of hydroxyl radicals. On the positively charged Ca-incorporated titanium, the negative ions of phosphate in body fluid are absorbed due to electronic charge attraction.[36] As the more phosphate ions are absorbed on the surface, the more calcium ions are attracted on the surface, which consequently forms a great amount of calcium phosphates. According to the authors, Ca ions are gradually released from the surface of the Ca-incorporated titanium. The gradual release of Ca ions accelerates the precipitations of calcium phosphate on the surface, which possibly resulted in the rapid bone formation of the Ca-incorporated implants compared to the non-incorporated cp titanium.

iii) Catalytic effect of bioactive chemistry on the bone integration to titanium surfaces: Ellingsen investigated the bone response to fluoride-treated titanium prepared by chemical etching in sodium fluoride (NaF).[5] The author found that NaF-treated implants showed greater retention in bone than non-treated cp titanium. The author suggested that "the presence of a fluoride coat on the surface of titanium stimulates the bone response leading to a connection between titanium and phosphate from tissue fluids". In addition, the author proposed that "free fluoride ions will catalyze this reaction and induce the formation of fluoridated hydroxyapatite and fluorapatite in the surrounding bone."

Despite of the rapid bonding ability of the bioactive implants in bone at early healing periods, however, several bioactive implants demonstrated adverse effects on the bone response after 1 or 2 years of healing due to biodelamination and biodegradation of thick coating materials[37], which possibly caused severe bone resorption around the implants, and finally resulted in the implant failure.[38] To overcome these possible risks of the biodegradation and biodelamination of bioactive materials on dental implants, several technologies have been applied to dental implant productions by coating bioactive materials at the nanometer scale or by incorporating the bioactive ions into titanium oxide layer. Surface chemistry-modified titanium/titanium alloy implants are now commercially available in the world market.

1.3 Surface Chemistry of Commercially Available Clinical Implants

Clinical implants have been manufactured by various surface engineering techniques including chemical treatments, physical modifications and different hybrid methods.[8,9,12,39-43] Depending on the engineering techniques, surface properties of dental implants show great differences in surface chemistry, topography, oxide thickness and crystal structure. In particular, surface chemistry of clinical implants is determined by the experimental conditions of surface engineering processes.[44-47] In this section, the surface chemistry of several commercially available dental implants is summarized depending on their engineering techniques (Surface chemistry of the clinical implants is referenced from XPS data of previous studies.)

Electrochemical oxidation: The electrochemical oxidation technique is an electrolytic passivation process, known as an anodizing or micro arc oxidation method (MAO). The electrochemical oxidation used on several clinical implants not only creates porous structures on the surfaces, but also incorporates cations and anions from the electrolytes used. Furthermore, these implants can contain great amounts of hydroxyl groups on surface as compared to commercially pure titanium due to anodic reaction, e.g; $Ti^{4+}(ox) + 4H_2O(aq) \rightarrow Ti(OH)_4(ox) + 2H_2 \rightarrow TiO_{2-x}(OH)_{2x} + (2-x)H_2O$.[48]

TiUnite from Nobel Biocare: The TiUnite implant is manufactured by an electrochemical oxidation technique using a P-containing mixed electrolyte.[49] The implant surface contains 7% of phosphorous in titanium oxide.[44] The chemical bonding state of P is mainly titanium phosphates.

M implant from Shinhung: The M implant is produced with an MAO method using a Mg-containing mixed electrolyte. The M implant surface contains Mg ions (≤ 9.3%) and P ions (≤ 3%) in titanium oxide.[12] The chemical bonding state of Mg is mainly composed of magnesium titanates.

Ospol implant from Ospol: The Ospol implant is prepared with an MAO method using a Ca-containing mixed electrolyte. The Ospol implant contains Ca ions (< 11%) in titanium oxide.[9] The chemical bonding state of Ca in titanium oxide is mainly calcium titanates.

Acid etching: The acid etching technique is one of subtractive methods for altering titanium surfaces. In general, acid etching forms various micro- and nano-structured surfaces whereas surface chemistry of titanium seldom changed after acid etching.[44]

Osseotite from BIOMET *3i*: The Osseotite implant is manufactured by a dual acid etching process: The implant are soaked in HF solution, and then chemically etched in a mixture of HCl/H_2SO_4, and finally heat treated at 60-80°C for 3-10min.[50] The main chemical compositions of the Osseotite are Ti, O and C. The possible remnants of Cl, S and F were not or negligibly detected at the Osseotite implants.[44,46]

OsseoSpeed from Astra Tech AB: The OsseoSpeed implant is produced by grit-blasting with TiO_2 particles and acid etching including diluted hydrofluoric acid.[15,50] The surface chemistry of the OsseoSpeed is mainly composed of Ti, O and C. In addition, the OsseoSpeed implant contains small amounts of F (0.3-0.5%).

SLA implant from Straumann: The SLA surface is blasted with large grits of Al_2O_3, and then chemically etched in a mixture of H_2SO_4/HCl.[51] The SLA implant shows crystallographically oriented etching pits. The surface chemistry of SLA implants is mainly composed of Ti, O and C. Alumina residuals from the grit-blasting process are often detected on the SLA implant.[44,46]

Plasma spraying: The plasma spraying technique represents a coating process by spraying thermally melted materials on implant surfaces.[4] The thermal spraying technique generally forms thick layer of plasma materials, such as hydroxyapatite and titanium. The plasma spraying technique has been applied to dental implant productions for creating bioactive surfaces with hydroxyapatite coating as well as for roughening implant surfaces by titanium plasma coating.

TPS implant from Straumann: The TPS implant is produced by titanium plasma spraying (TPS) technique. The surface chemistry of the TPS implant is mainly composed of Ti, O and C including small amounts of N.[46] The chemical bonding states of Ti and O is mainly TiO_2, while N is detected as titanium nitrates due to thermal heating during TPS process.

Steri-Oss HA-coated implant from Nobel Biocare: The Steri-Oss implant is coated with hydroxyapatite using plasma spraying technique.[52,53] The surface chemistry of the Steri-Oss implant is mainly composed of Ca, P and C. The amount ratio of Ca and P is 1.62 (Ca/P = 17.7/10.8).[52] The top layer (1-2 μm) of HA-coating materials is amorphous, but the rest layer shows the crystal structure of hydroxyapatite (hexagonal packed HA phase).[53]

Sol-gel technique: The sol-gel process is one of wet-chemical techniques using chemical solutions which lead to gel formation on sample surface, such as discrete particles or network polymer.[54] In general, heat treatments follow after gel formation on the surface to enhance the mechanical stability of gel structure. By controlling soaking time, chemical solutions and heat treatments, the sol-gel process enables change of surface chemistry and topography of titanium surfaces from micro to nanoscale.

Nanotite from BIOMET *3i*: The Nanotite implant is produced by discrete crystalline deposition of calcium phosphates onto a dual acid etched surface.[16] The Nanotite surface is covered with

calcium phosphate particles of 20-100 nm in size. Surface chemistry of Nanotite is composed of Ti, O, C, Ca and P. The concentration ratio of Ca and P is ≈ 2.1(Ca/P = 10.62/5.01) .[55]

Ion-beam assistant deposition (IBAD) technique: The IBAD technique is one of dry methods to deposit thin films of source materials onto a substrate. The IBAD technique enables formation of a thin film of bioceramic, such as hydroxyapatite and calcium phosphate on dental implants. The film thickness ranges from several tens of nanometers to several micrometers depending on the experimental parameters.[56]

Integra CP/NanoTite from Bicon: The Bicon implant is manufactured using an ion beam assistant bioceramic deposition on Ti-6Al-4V surfaces.[57] Yet, no XPS data of this clinical implant is available on Pubmed database except that experimental implants prepared by the IBAD technique of the Bicon company showed the presence of O, C, Ca, P and Al on the implant surfaces.[58] The concentration ratio of Ca and P at the experimental implants ranged from 1.2 to 2.2 on the as-received surfaces.[58]

Blasting technique: Grits-blasting techniques have been widely applied to dental implant productions during last two decades to increase the roughness of titanium surfaces. Since the blasting particles are collided with implant surfaces, debris and residuals of the blasting particles are often found on the blasted surfaces in SEM observations.[44,46] Surface chemistry analysis confirmed the presence of blasting residuals on the blasted surfaces.[46]

TiOblast from Astra Tech AB: The TiOblast surface is produced by grit-blasting of TiO_2 particles on cp titanium. The surface chemistry of the TiOblast implant is mainly composed of Ti, O and C including trace levels of N and Na.[59]

Ossean from Intra-Lock, FL, USA: The Ossean surface is produced by blasting of RBM particles (bioceramic particles composed of Ca and P) on Ti-6Al-4V implant.[60] Main elements of the Ossean surface are Ti, O, C, Al, Ca and P including small amounts of N and Si. The concentration ratio of Ca and P is 0.16 (Ca/P = 0.5/4.0).

1.4 Surface Chemistry Modifications of Titanium Surfaces

Surface chemistry modifications of titanium implants in the present thesis are performed using metal plasma immersion ion implantation (MePIIID) and micro arc oxidation processes. These techniques can incorporate 'bioactive ions', such as Mg, Ca, P and Na, into titanium surfaces without forming weak and thick coating layers, which may results in implant failure due to biodegradation and biodelamination of the coating materials. Furthermore, MePIIID process allows surface chemistry modification with negligible alteration of surface topography at the nanometer level, thus enabling the investigation of the effect of bioactive implant surface chemistry on the bone response. The details of these processes are described in the following subsections (see 1.4.1 and 1.4.2).

Among many candidates of bioactive titanium surfaces, Mg- and Ca-incorporated

implants were selected in the present thesis to investigate the effect of surface chemistry on the bone responses to titanium. According to Sul and colleagues, Mg- and Ca-incorporated titanium surfaces significantly reinforced the bonding strength and speed of the implants in rabbit bone compared to non-incorporated pure titanium.[11,12] One plausible explanation for the enhanced bone responses to Mg- and Ca-incorporated titanium is that surface chemistry mediated-osseointegration via "electrostatic/ionic" bonds, namely biochemical bonding, occurs at the bone-implant interface.[11,61] Because Mg and Ca cations in titanium oxide provide numerous binding sites for the attachments of adhesive bone matrix proteins, Mg and Ca ions in titanium surfaces may electrostatically bond with polyanionic proteins, such as proteoglycans, collagen, thrombospondin, fibronectin, vitronectin, fibrillin, osteoadherin, osteopontin and bone sialoprotein.[33-35] This process can stimulate the Arg-Gly-Asp (RGD) sequence and trigger further recruitment of osteoprogenitor cells and osteoblasts via signaling pathways, which possibly leads to rapid and strong bone formation at Mg- and Ca-incorporated titanium.[11,62]

1.4.1 Plasma Immersion Ion Implantation and Deposition (PIIID)

Plasma ion implantation technique has been known as plasma source ion implantation (PSII) or plasma based ion implantation (PBII) since non-condensable gaseous plasmas (O, N, Ar, etc) were generally employed to this technique.[63] However, after condensable plasma species (metal plasma of Mg, Ca, Fe, Ti, etc) were applied to this technique[64,65], plasma ion implantation technique is generally known as plasma immersion ion implantation & deposition (PIIID) due to the repeated-phases of ion implantation and deposition; ion implantation phase during bias pulse on and deposition phase during bias pulse off.[63] In the present study, PIIID is used as general terminology for plasma ion implantation techniques and divided into two categories: MePIIID for metal arc plasma and O PIIID for gaseous plasma of oxygen. MePIIID is often described as Mg PIIID and Ca PIIID depending on the used plasma source.

MePIIID process is a cyclic process of repeating cathodic arc deposition and plasma immersion ion implantation.[64,66] Alternations of implantation and deposition of plasma ions finally forms the intermixed layer between the substrate and film during the MePIIID process[67, 68], which leads to excellent mechanical properties with the benefit of preventing biodelamination and biodegradation of implant surfaces in bone.[69,70]. MePIIID takes advantages to overcome the line-of-sight restriction inherent in conventional ion implantation[63], enabling application of homogeneous film formation of complex geometry samples including screw-shaped implants. Furthermore, MePIIID allows surface chemistry modification with negligible alteration of surface topography at the nanometer level thus enabling the investigation of the effect of bioactive implant surface chemistry on the bone response.[31] By tailoring plasma sources and ion dose, MePIIID can create desired bioactive surface chemistry for a better understanding of osseointegration mechanism.

O PIIID process is a periodic plasma ion implantation process of oxygen plasma.[63] Under 0.1 Pa of oxygen pressure, an energetic negative bias generates gaseous plasma and accelerates

the plasma ions into the normal direction of titanium surface, thus allowing homogeneous incorporation of plasma ions into the implants. O PIIID process can be performed under the same ion dose and acceleration voltage used on MePIIID process.

The present thesis investigated the effect of MePIIID process parameters, i.e., plasma sources of magnesium and calcium, ion dose, and acceleration voltage on the surface chemistry and morphology of screw-type titanium implants that have been most widely used for osseointegrated implants. Furthermore, we investigated the bone response to plasma immersion ion implantation and deposition of titanium implants with oxygen and magnesium.

1.4.2 Micro Arc Oxidation (MAO)

MAO process is an electrolytic passivation process, known as electrochemical oxidation or anodic oxidation process. By controlling the process parameters, such as current density and electrolytes, the MAO process may modify the surface properties of titanium oxide, including surface morphology, chemistry, oxide thickness, roughness and crystal structure.[21,71,72] According to previous studies, the MAO process not only produced porous structures on titanium surfaces by dielectric breakdown phenomenon, but also incorporated anions and cations from the electrolytes used.[71] Although the ion incorporation into titanium oxide during the MAO process is not fully understood, Sul et al produced Mg-, Ca-, P- and S-incorporated titanium surfaces.[9,11,32] With respect to the mechanical strength of the oxidized layer, the ultimate tensile strengths of the oxidized surfaces prepared with anodic oxidation process were higher than the ultimate tensile strength of cp titanium surfaces when the dielectric breakdown occurred: the ultimate tensile strength was 32.8 MPa for the cp titanium, 34.2 MPa for the titanium anodically oxidized with the dielectric breakdown, and was ranged from 13.1 to 20.2 MPa for the titanium anodically oxidized without the dielectric breakdown.[73] This result, indeed, confirm the mechanical stability of Mg- and Ca-incorporated titanium oxides prepared with the MAO process. TiUnite from Nobelbiocare, Ca implant from Ospol and M implant from Shinhung are commercially available dental implants manufactured by MAO process.

In the present thesis, Mg- and Ca-incorporated titanium implants were produced with the MAO process and their outcomes in rabbit tibiae were investigated.

1.5 Surface Characterization Methods

1.5.1 X-ray Photoelectron Spectroscopy (XPS)

Since Einstein explained the principle of photoelectron emission from metal substrates, the photoelectronic effect has been applied to the analytical tools for the investigation of electron energy states in materials. The photoelectronic effect can be described as following simple equation: $E_k = h\upsilon - E_B - W$, where E_k is kinetic energy of photoelectron, $h\upsilon$ is the photon energy, E_B is binding energy of the electron, and W is work function of materials.[74] XPS is one of analytical tools based on the photoelectronic effect for the analyses of surface chemistry and

electronic band structures of materials using X-ray sources. Al Kα ($h\upsilon$ = 1486.7eV) and Mg Kα ($h\upsilon$ = 1253eV) lines are generally used for X-ray source.[75,76] By measuring the kinetic energy of photoelectrons, we can investigate the electron binding states, namely chemical bonding states, of materials. Fig. 1 illustrates the photoelectric effect and XPS measurement. For a precise analysis of surface chemistry, the binding energy should be referenced with a reference material (Cu, Ag) or hydrocarbon on the surface to compensate the charging differences from materials to materials. In the present thesis, all XPS data have been referenced by hydrocarbon of 284.8eV.[77] XPS provides the quantitative analysis of surface chemistry. By using the signal intensity and sensitivity factor of elements investigated, we can know the relative atom concentration of surface chemistry. The quantitative accuracy is about 80-95% depending on the experimental conditions and signal intensities of elements.[77] Since the detection limit of XPS is several tenths of nanometers into the surface, XPS provides very sensitive and reliable information on the surface chemistry. However, the lateral resolution of XPS is in the range values of 100-500 μm. The advantage of XPS is to analyze surface chemistry with X-rays which are less damaging to the surface than electron beams of AES and ion beams of SIMS.[76]

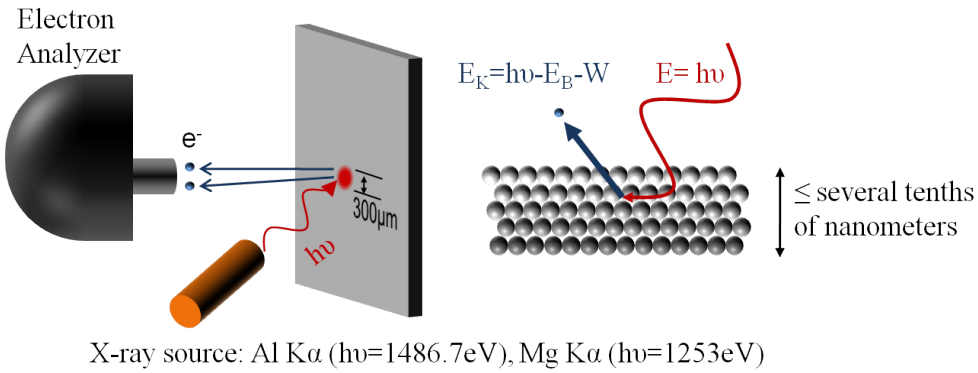

Fig. 1. The illustration of XPS measurement and the photoelectric effect

1.5.2 Auger Electron Spectroscopy (AES)

Auger electrons are produced when the electron bombardment makes an atomic inner shell vacancy.[75] During an electronic rearrangement due to the filling process of the vacancy, electrons from outer shells are emitted from the surface and provide the chemical composition as well as chemical bonding states of surface elements.[76] In addition, with use of continuous Ar^{2+} etching, we can investigate the elemental distribution in depth, namely depth profile. Although AES is a more destructive method of surface analysis than XPS and does not provide the electronic bonding state of an inner shell[76], AES is widely used for surface chemistry analyses due to its' higher spatial resolution (< 100 nm) than that of XPS. In the present study, AES was employed for depth profiles of elements near the surface region.

1.5.3 Scanning Electron Microscopy (SEM)

SEM is an analytical tool measuring surface topography using energetic electron beams. The electron beam can be focused by a magnetic field from micro to nanometer level, thus enabling measurement of surface topography at the magnification of × 10 to × 500,000.[76] SEM provides images of secondary electron (SE) or back scattered electron (BSE) modes. In general, the SE mode mainly supplies images based on the topographical information, while the BSE mode can provide the mixed information of topography as well as composition. Compared to the BSE mode, high-resolution images (≥ × 10,000) of samples can be achieved at the SE mode.

1.5.4 Optical Interferometry

Optical interferometry is one of methods to measure surface topography based on the interference phenomenon between on-going light from a source and reflected light from a surface. The intensity differences of the interfered lights transform to the height difference of surfaces, which allows the measurements of surface roughness. In general, an interferometer measures surface topography using a white light source which has a wave length of 300-800 nm. Due to this wavelength, the lateral resolution of an interferometer is over 100 nm.[78] In contrast to the lateral resolution, an optical interferometer has a vertical resolution of less than 1 nm.[78] One of important factors in the roughness measurement is the measuring area. Since dental implants do have heterogeneous topographies, the roughness value depends on the size and the macro geometry of local areas where the measurements were performed. Furthermore, as-received roughness values of dental implants contain the information of complex geometry of screw design, so-called "waviness" or "error form". To remove the waviness and error forms of samples, Gaussian filtering is generally used. However, the surface roughness values, particularly Sa value, depends on the filtering size: the Sa value increases with filtering size.[79,80] In the present thesis, the surface roughness was measured from thread-tops, thread-flanks and thread-valleys of implants, and then the roughness values were statistically compared between implant groups. The measuring area of 230 μm × 230 μm and a Gaussian filter of 50 μm × 50 μm were used for surface roughness comparisons.

1.6 Bone/Cell Responses to Surface Chemistry-modified Titanium/Titanium Alloys

1.6.1 Magnesium-incorporated Titanium/Titanium Alloy Surfaces

In vivo

Sul et al 2005[32] investigated the bone integration of Mg-incorporated implants prepared with the MAO process. The concentration of Mg ions on the Mg-incorporated implant was 7.58% prior to insertion, while Mg ions were not detected on the retrieved implants after 6 weeks of healing in rabbit femur. The Mg-incorporated implants revealed significantly higher removal torque (RTQ) and interfacial stiffness (ISQ) values than non-incorporated cp titanium.

Sul et al 2005[81] investigated the optimum surface properties of oxidized implants for the reinforcement of the osseointegration using Mg-incorporated implants. The Mg-incorporated implants were prepared by the MAO process with different experimental parameters, thus containing four different Mg concentrations ranged from 8.36% to 9.33%. The Mg-incorporated titanium implants presented significant increase of removal torque as compared to non-incorporated cp titanium. In addition, the removal torque value of the Mg-incorporated titanium increased with Mg concentration. The authors concluded that the Mg concentration of optimal oxidized implants is approximately 9% in relative atom concentration.

Sul et al 2005[61] investigated the effect of Mg-incorporation to titanium oxide on the osseointegration of implants. The implants prepared with the MAO process contained ≤ 9.3% of Mg. Removal torque tests presented significantly higher bonding strengths of the Mg-incorporated implants in rabbit tibia compared to non-incorporated cp titanium. EDX line profiles at the bone and implant interface revealed the ion exchange of Mg, Ca and P ions between the implants and surrounding bone tissue. The authors concluded that these results provide positive evidences for surface chemistry-mediated "biochemical bonding theory" of oxidized implants.

Sul et al 2006[82] investigated the bonding strength and speed of Mg-incorporated implants in rabbit tibiae. The implants were prepared with the MAO process and contained 9.3% of Mg. The Mg-incorporated titanium showed significantly higher removal torque values than cp titanium controls at the healing times of 3 and 6 weeks. The osseointegration speed, defined as ΔRTQ/Δhealing time (Ncm/week), was 3.4 Ncm/week for Mg-incorporated implants and 2.6 Ncm/week for cp titanium controls, which showed a significant difference in Wilcox-signed rank test. The authors concluded that Mg-incorporated implants were rapidly and strongly integrated in bone.

Sul et al 2006[12] compared the strength and speed of osseointegration among three groups of implants, such as Mg-incorporated titanium implants prepared with the MAO process, TiUnite implants from Nobel Biocare and Osseotite implants from BIOMET *3i*. The Mg concentration of the Mg-incorporated implants was ≤ 9.3%. The Mg-incorporated implants showed a significantly higher RTQ value than the two clinical implants at a healing time of 3 weeks. After a healing time of 6 weeks, the Mg-incorporated implants revealed a significantly higher RTQ value than the Osseotite implants, but showed only a higher value than the TiUnite implants. The speed of osseointegration was significantly faster for the Mg-incorporated implants and for the TiUnite implants between 3 and 6 weeks of healing time, but was not significantly fast for the Osseotite. The authors concluded that surface chemistry facilitated the strong and rapid osseointegration of the Mg-incorporated implants.

Sul et al 2009[29] investigated the bonding speed and strength of Mg-incorporated implants prepared with the MAO process. Magnesium was detected less than 9.17% on the Mg-incorporated implants. The Mg-incorporated implants showed significantly higher removal torque values than machined-turned cp titanium implants and Al_2O_3-blasted implants after 3 weeks and 6 weeks of healing whereas the blasted implants presented significantly higher RTQ

values than the machined turned implants after 6 weeks of healing. The Mg-incorporated implants revealed a significantly higher rate of osseointegration as compared to the machined-turned and the blasted implants between 3 and 6 weeks of healing time.
Sul et al 2010[31] investigated the integration strengths of Mg-incorporated implants and O-incorporated implants in rabbit tibiae by measuring the tensile strength. Magnesium and oxygen ions were incorporated into titanium surfaces using PIIID techniques. The Mg-incorporated implants presented a significantly higher tensile strength than the O-incorporated implants.

In vitro
Park et al 2010[83] investigated *in vitro* osteoconductivity of Mg-incorporated titanium prepared with hydrothermal treatment. The hydrothermal treatment was performed on two different micro-structured surfaces of abraded minimally rough titanium and grit-blasted moderately rough titanium. The incorporated Mg ion was ≈ 7.1% for the minimally rough titanium and 6.3% for the moderately rough titanium. The Mg incorporation significantly increased the attachment of MC3T3-E1 (pre-osteoblast cell) on the minimally rough titanium, while the Mg-incorporation had negligible influences on the cellular attachment of the moderately rough titanium. The Mg-incorporation enhanced ALP activity of cells cultured on the minimally and moderately rough titanium surfaces. Furthermore, the Mg-incorporation increased the mRNA expressions of the osteoblast genes and integrins in cells grown on the minimally and moderately rough surfaces.

Zreiqat et al 2005[62] investigated the effect of surface chemistry modification of Ti-6Al-4V with magnesium on the regulation of key intracellular signaling proteins in human bone-derived cells (HBDC). The Mg-incorporated Ti-6Al-4V was prepared with an ion implantation process. After 2 hours of the cell culture, the Mg-incorporated surfaces revealed higher expression levels of β1-integrin, Shc isoforms (pp66, p52, p46), phosphorylated Erk and c-fos protein in cells compared to non-incorporated titanium alloy. They found that the Mg-incorporated titanium alloy modulated key signaling proteins such as Shc; a common point of integration between integrins and the Ras/Mapkinase pathway. Furthermore, the signaling pathway involving c-fos was upregulated in the osteoblasts cultured on the Mg-incorporated surfaces. The authors concluded that surface chemistry modifications of titanium alloy with magnesium may lead to successful osteoblastic function and differentiation.

1.6.2 Calcium-incorporated Titanium/Titanium Alloy Surfaces

In vivo
Hanawa et al 1997[18] investigated the bone response to Ca-incorporated titanium in rat tibiae. Using an ion implantation process, the Ca ions were implanted into an upper side of cp titanium plates at a dose of 10^{17} ions/cm^2, while the other side (lower side) was not treated with the ion implantation. Decalcified cut and ground sections displayed a greater amount of new bone formation at the Ca-incorporated titanium side than at the non-incorporated side after 2 days of

healing. In addition, tetracycline labeling was observed on the Ca-incorporated side of the titanium plates, but not observed on the non-incorporated side of the titanium plates after 8 days of surgery. The authors concluded that the Ca-incorporated titanium may be superior to the non-incorporated cp titanium for bone conduction.

Sul et al 2002[39] investigated the bone response to Ca-incorporated implants prepared by the MAO process. The relative atom concentration of Ca was approximately ≤ 11%. The Ca-incorporated implants demonstrated significantly higher removal torque values and bone metal contact % than non-incorporated cp titanium after 6 weeks of healing in rabbit tibiae. The authors concluded that surface chemical composition of titanium implants play an important role on the bone responses.

Sul 2003[9] compared the strength of osseointegration between Ca-, P-, S-incorporated implants and non-incorporated cp titanium using a rabbit model. The Ca-incorporated implants were prepared with the MAO process and contained approximately ≤ 11% of Ca. The Ca-incorporated implants presented significantly higher removal torque as compared to the non-incorporated titanium implants and the P-incorporated implants whereas no significant differences were found between the removal torque of the Ca-incorporated implants and the S-incorporated implants. In addition, the Ca-incorporated implants showed a significantly greater bone metal contact% than the non-incorporated cp titanium. The author concluded that surface chemistry and topography separately or together play important roles in the bone response to oxidized implants.

Sul et al 2004[11] investigated the effect of calcium chemistry of oxidized implants on the implant integration in rabbit tibiae. The MAO process was used to produce Ca-incorporated implants (Ca 7.37% on the as-received surface). The Ca-incorporated implants showed significantly higher removal torque values than non-incorporated cp titanium (27.6 vs 8.8 Ncm, 314% increase) after 6 weeks of healing time. The authors have suggested two action mechanisms of the strong and fast bone integration to the Ca-incorporated implants: (1) biomechanical interlocking through bone growth in pores and (2) biochemical bonding.

Park et al 2007[84] evaluated the biocompatibility of Ca-incorporated Ti6Al4V alloy implants produced by hydrothermal treatment. The thickness of Ca-incorporated TiO_2 layer ranged from ≈ 250 nm to ≈ 1200 nm depending on the mol concentrations of NaOH and CaO used. The Ca-incorporated implants presented significantly higher removal toque values (3.2 vs 2.2 Ncm) and bone metal contact % (36.7 vs 20.2%) than the non-incorporated cp titanium. The authors concluded that the Ca-incorporation to TiO_2 layer may be an effective tool for improving the biocompatibility of Ti6Al4V implants.

Fröjd et al 2008[85] compared the osseointegration between Ca-incorporated implants, oxidized titanium implants and Al_2O_3 grit-blasted implants using a rabbit model. The Ca-incorporated implants and the oxidized implants were prepared with the MAO process. The Ca-incorporated implants contained ≈ 11% of Ca. Despite significantly lower Sa value of the Ca-incorporated implants compared to the other implants, the Ca-incorporated implants showed the significantly highest bone implant contact %. According to the authors, one reason for this can be explained by that a certain chemistry of titanium implants is of importance for bone attachment.

In vitro

Krupa et al 2001[86] investigated the corrosion resistance of Ca-incorporated titanium surfaces in SBF solution and the cell (human derived bone cells) responses to the Ca-incorporated titanium. The Ca-incorporated titanium produced by an ion implantation process contained 1.5% of Ca. Under stationary conditions, the Ca-ion implantation increased the corrosion resistance of titanium surfaces. From XTT assay and measurements of alkaline phosphatase (ALP) activity, the Ca-incorporated implants showed similar viability and ALP activity of osteoblasts as compared to non-incorporated cp titanium (grade2).

Nayab et al 2005[87] investigated the effect of Ca-implantation to titanium on the attachment and spreading of MG-63(osteogenic sarcoma cell). Using ion implantation methods, Ca ions were implanted into titanium at three different dose levels (10^{17}, 10^{16}, 10^{15} ions/cm^2). At the initial stages of cell culture (4 hours), the Ca-implantation to titanium with the highest dose enhanced the spreading of MG-63 cells, but inhibited the cell attachment. With increasing the culturing time, cell adhesion to the Ca-incorporated titanium with the highest dose significantly increased and more so than non-incorporated cp titanium. The authors suggested the possibility that "the sufficient Ca ions in titanium might trigger enhanced binding of the integrin receptor, thereby stimulating integrin-mediate activation signaling pathway".

1.6.3 Phosphorous-incorporated Titanium Surfaces

In vivo

Sul et al 2004[9] investigated the bone response to P-incorporated titanium implants. The P-incorporated implants were prepared with the MAO and inserted in rabbit tibiae for 6 weeks. The P-incorporated implants showed higher removal torque value than non-incorporated cp titanium, but not significantly different. The bone metal contact % was significantly higher for the P-incorporated implants compared to the non-incorporated cp titanium. The authors presented that the greater bone response to the P-incorporated implants can be explained by chemical reactions of phosphate titanium oxide with bone tissue.

Omar et al 2011[88] compared the bone tissue response between P-incorporated titanium implants (TiUnite, Nobel biocare, Sweden) and non-incorporated cp titanium. Phosphorous was detected about 3.6% at the the P-incorporated surface. The bone bonding strength was measured by a removal torque test 6, 14 and 28 days after implant insertion in rat tibiae. The P-incorporated implants showed significantly higher removal torque than the cp titanium after 6, 14 and 28 days of healing time. Furthermore, the P-incorporated implants only significantly increased the removal torque value with healing time, while the removal torque slightly increased with healing time for the non-incorporated cp titanium. From gene expression analyses, the authors found that the downregulation of gene expression of proinflammatory maker and upregulation of marker for bone formation and remodeling were presented on the P-incorporated implants.

In vitro

Krupa et al 2002[89] investigated the effect of phosphous-ion implantation on the corrosion resistance and biocompatibility of titanium. The P-incorporation at a dose of 1×10^{17} increased the corrosion resistance of titanium. The P-incorporated titanium presented no significant difference in XTT viability assay and ALP activity test compared to non-incorporated titanium.

1.6.4 Fluorine-containing Titanium Surfaces

In vivo

Ellingsen 1995[5] investigated the bone response to fluoride-treated titanium. The fluoride-treated implants were prepared by soaking in two different concentrations of sodium fluoride, 0.5% NaF and 4% NaF. The bone bonding strength was measured by a push out test 4 weeks and 8 weeks after the implant insertion in rabbit ulna. The NaF-treated implants showed greater retention in bone than non-treated cp titanium. Furthermore, the 4%NaF-treated titanium seemed to give higher retention than 0.5% NaF-treated titanium. The author suggested a catalytic effect of F ions on the bone response, which leads to a connection between titanium and phosphates from bone tissue.

Ellingsen 2004[15] investigated the effect of a fluoride modification of titanium surfaces on subsequent bone responses. The fluoride modification was performed on TiO_2 grit-blasted implants using a diluted hydrofluoric acid. Despite slightly lower Sa values, the fluoride-modified implants showed significantly higher removal torque values, shear strengths and bone metal contact % than non-treated blasted implants at 3 months after placement in rabbit cortical bone. The author suggested the possibility that the modified surface chemistry and small morphologic changes (small etching pits) of the fluoride-treated surfaces have a beneficial effect on the bone healing.

Lamolle et al 2009[90] investigated the bone attachment strength to F-incorporated titanium implants prepared by a cathodic reduction process in HF containing electrolytes. The concentrations of HF in the electrolytes were 0.0011, 0.01 and 0.1vol%. The bone attachment strengths were measured by pull-out tests 4 weeks after implant insertion in rabbit tibiae. The bone-to-implant attachment strength increased with atom concentration of F near surface ($\leq$ 30 nm). The attachment strength positively correlated with the amounts of F^- and H^+. According to the authors, these results supported the idea that chemical elements, such as fluoride or hydride, can be useful for improving the biological response to titanium surfaces.

Sul 2010[10] compared the osseointegration between TiO_2 grit-blasted titanium implants and fluorinated TiO_2 nanotube implants. The fluorinated nanotube implants were fabricated by an electrochemical oxidation process in the mixture of H_3PO_4 and HF. The F ion concentration on the fluorinated nanotube implants ranged from 4.0% to 4.6% depending on the processing time. The fluorinated implant containing 4.6% of F was selected for an animal study. Despite of significantly lower Sa and Sdr values, the fluorinated nanotube implants demonstrated the higher removal torque values and bone metal contact percentages than the blasted titanium surfaces at 6

weeks after placement in rabbit femur condyle region. The author concluded that the presence of the nanotube and the fluorinated surface chemistry determined the nature of bone responses to the implants.

In vitro

Lamolle et al 2009[91] investigated the surface chemistry, topography and biocompatibility of titanium surfaces treated with 0.2% HF acid. The murine osteoblasts (MC3T3-E1) were cultured on a polished control group and test groups treated with HF acid at different exposure times (40s, 90s, 120s and 150s). For short treatment times (40s, 90s), the fluorine was detected within 5 nm from outermost surface, while the fluorine was incorporated deeper for longer treatment times (120s, 150s). The cytotoxicity level measured by LDH activity was found lower for all the HF-treated titanium surfaces compared to the polished titanium control, and the levels were significantly lower for the HF-treated surfaces with the longer treatment times. Numbers of cell attached on the HF-treated surface with the longer treatment times were significantly higher compared to the control group.

1.6.5 Hydroxyapatite-/Calcium Phosphates-containing Surfaces

In vivo

Gottlander et al 1997[37] investigated the bone response to hydroxyapatite (HA)-coated titanium implants. The HA coating thickness was approximately 51 µm with a plasma spray process. The HA-coated implants showed significantly higher bone contact % compared to non-coated cp titanium at 4 weeks and 6 months after implant insertion in rabbit bone. However, as compared to the cp titanium implants, the HA-coated implants showed significantly lower bone area % inside threaded area and outfolded mirror area after 6 months of healing time. According to the authors, small amounts of bone adjacent to the HA-coated implants could be explained by macrophage-induced resorption.

Ishizawa et al 1995[92] compared the bone response of anodically oxidized titanium, anodically oxidized + hydrothermally treated titanium, non-treated cp titanium and sintered HA ceramics. The anodic oxidation process was performed on cp titanium implants in mixed electrolytes (sodium β-glycerophosphate and calcium acetate), and the process finally formed an anodic titanium oxide film containing Ca and P (AOFCP). The hydrothermal process was performed at 300°C for 2 hours using an autoclave with water, which finally formed numerous hydroxyapatite crystals on the AOFCP surface. The anodically oxidized titanium and the anodically oxidized + hydrothermally treated titanium presented significantly higher interfacial shear strength and bone apposition % than the non-treated cp titanium 8 weeks after the implants insertion in rabbit femur. However, there were no significant differences in the shear strength and bone apposition % between the sintered HA and the anodically oxidized + hydrothermally treated titanium. The author found that thin HA layers, only a few micrometers thick, may be sufficient for implants to acquire the abilities of bioactive materials.

Geesink et al 1988[93] investigated the bonding strength of hydroxyapatite-coated titanium implants in dog femur. The hydroxyapatite-coated implants were prepared with a plasma-spraying technique. The hydroxyapatite-coated implant showed significantly increased interfacial shear strength compared to non-coated cp titanium after 6 weeks of healing time. The shear strength increased with healing time up to 6 months, but slightly decreased after 1 year follow-up. The authors concluded that the hydroxyapatite-coated implant can form a chemical fixation in bone, which strength is comparable to the mechanical strength of cortical bone itself.

Ong et al 2002[94] compared the bone responses to CaP-coated titanium, CaP-coated & heat-treated titanium and non-coated cp titanium implants. Radio frequency (RF) sputtering process was used for the CaP coating on titanium surfaces and the heat treatment was performed under 700°C for 90min. As compared to the non-coated cp titanium and the CaP-coated & heat-treated implants, the CaP-coated implants revealed significantly higher interfacial shear strength 3 weeks after the implants insertion in dog, while the shear strengths of the implants became similar after 12 weeks of healing time. Furthermore, the CaP-coated implants presented significantly greater % of bone implant contact than the other two implants after 3 weeks and 12 weeks of healing. The author suggested that the dissolution of the CaP coatings may play a important role in the enhanced bone response to the CaP-coated titanium.

Siebers et al 2007[95] investigated the bone response to CaP-coated titanium implants prepared with an electrostatic spray deposition (ESD) and heat treatment process. After titanium implants were coated with CaP using the EDS process (coating layer ≈ 2μm), the implants were subjected to an additional heat treatment at three different temperature conditions (400°C, 500°C and 700°C) for 2 hours. Depending on the temperature during the heat treatment, the implants revealed different crystallinity of amorphous structures for 400°C, carbonate apatite structure for 500°C and carbonated hydroxyapatite structure for 700°C. After 12 weeks of implant insertion in goat femur, the CaP-coated implants having carbonated hydroxyapatite crystalline presented a significant increase of bone metal contact % compared to non-CaP coated cp titanium implants, while two other CaP-coated implants showed no significant difference of bone metal contact % compared with the cp titanium implants. The author concluded that the degree of crystallinity has an influence on the bone response to CaP-coated implants prepared with the ESD process.

Mendes et al 2007[16] investigated the effect of discrete calcium phosphate nanocrystals on bone response to titanium/titanium alloy implants. The cp titanium and Ti6Al4V implants were dual-etched with acid and, then modified by a discrete calcium phosphate deposition process. The implants were bilaterally inserted in distal metaphyses of rat femora. After 9 days of healing, the discrete calcium phosphate deposition significantly increased the bone bonding strength to the titanium implants.

Quaranta et al 2010[96] compared the bone response of plasma-sprayed calcium-phosphate (PSCaP) implants and bioceramic nano-coated (Nano) implants prepared with an ion beam-assisted deposition process. The PSCaP coating and bioceramic coating were performed on TiAl64V implants (Bicon, Bodton, MA). After the ion beam-assisted deposition process, the Nano implants showed 300-500 nm thickness of CaP layer on the surface, while the PSCaP

surface presented 20-30µm thickness of CaP coating layer. The PSCaP implants showed significantly higher percentages of bone metal contact and bone area than the Nano implants 20days, 30days and 60days after the implants insertion in rabbit femur. The author concluded that the early bone response was favored by the presence of the thicker PSCaP coating.

In vitro

Fini et al 1999[97] investigated bone cell (HOS-TE85, human osteosarcoma line) responses to Ca- and P-incorporated titanium. Three different groups were used in this study: 1) HF-soaked cp titanium (Ti), 2) HF-soaked + anodically oxidized implants (Ti/Al), and 3) HF-soaked + anodically oxidized + heat-treated implant (Ti/Al/HA). Ca and P ions were incorporated into titanium after anodic oxidation and were enriched after the heat-treatment. Three surfaces presented no differences in cell morphology, vacuolation, detachment and membranelysis

Pham et al 2000[98] investigated the response of hydroxyapatite precipitation on Ca- and P-incorporated titanium using a simulated body fluid (SBF). The Ca- and P-incorporated titanium was prepared using an ion-implantation technique. The Ca- and P-incorporated titanium presented the enhanced precipitation and mineralization of the hydroxyapatite in the SBF compared to non-incorporated titanium. According to the authors, the encouraged surface reactivity was related to the increased provision of the ionic mineral components, such as Ca^{2+} and HP_4^{2-}, which act as nucleating cites for hydroxyapatite.

1.6.6 Sodium-containing Titanium Surfaces

In vivo

Nishiguchi et al 1999[99] investigated the effect of heat-treatment on the bone-bonding strength to alkali-treated titanium. The alkali-treated titanium was prepared by soaking in a 5M NaOH aqueous solution and the heat treatment was performed at 600°C for 1 hour. The alkali- and heat-treated titanium showed significantly higher detaching strength compared to non-treated cp titanium and the alkali-treated titanium (no heat-treatment) 8 weeks and 16 weeks after implant insertion in rabbit tibiae. The author concluded that a more stable sodium titanate layer was formed on the alkali-treated surface after heat treatment, which led to stronger bone bonding to the alkali- and heat-treated surface than to the alkali alone treated titanium.

Nishiguchi et al 1999[28] investigated the effect of alkali- and heat-treatment on the bone integration to three different titanium alloys. The alkali- and heat-treatment were performed to the titanium alloys of Ti6Al4V, Ti6Al2Nb1Ta and Ti5Mo5Zr3Al by soaking in NaOH containing aqueous solutions and subsequently heating at 550°C or 600°C for 1 hour. Detaching measurements showed that the alkali- and heat-treatment increased the bone-bonding strength of three different alloys 8, 16 and 24 weeks after implant insertion in rabbit tibiae. According to the authors, the titanium alloys bound chemically to bone via a crystallized sodium titanate layer formed by the alkali- and heat-treatment.

Fujibayashi et al 2001[100] investigated the effect of sodium removal on the bone bonding strength of alkali- and heat-treated titanium implants. For the sample preparation, cp titanium plates were soaked in 5M NaOH aqueous solution for 24 hours and were heated at 600 °C for 1 hour. Prior to the heat-treatment, sodium-free alkali- and heat-treated titanium (Na-free titanium) was prepared by an additional step of soaking in distilled water for 48 hours after the alkali treatment. At 4 weeks after implant insertion in rabbit bone, the Na-free titanium showed the significantly higher bone-bonding strength than the alkali- and heat-treated titanium. After 8, 16 and 24 weeks of healing times, the bone bonding-strength of the Na-free titanium negligibly changed whereas the alkali- and heat-treated titanium significantly increased the bone bonding strength with the healing time. As a result, the alkali- and heat-treated titanium showed significantly higher bone bonding strength than the Na-free titanium after 16 and 24 weeks. This reversal in the bonding strength between two groups was explained by the weakness of the surface structure of the Na-free titanium, which led the detachment between bioactive layer and bulk titanium.

In vitro

Maitz et al 2005[101] investigated the performance of osteogenic cells on Na-incorporated titanium prepared with three different methods, such as plasma immersion ion implantation & deposition (PIII&D), beam-line ion implantation (II) and wet chemical (NaOH-soaking) processes. After the PIII&D and II processes, the Na-incorporated implants were oxidized in air (1h at 600°C) and then hydroxylated in boiling water (2-4h). The precipitation of calcium phosphates in SBF was significantly higher for the PIII&D treated implants compared to the other implants. After 4-5 hours of cell culture, however, all four titanium surfaces (including non-treated cp titanium) showed similar cell adhesion and proliferation except that the implants prepared with NaOH-soaking process presented the best cell adhesion in the morphological aspects.

Baszkiewicz et al 2008[102] investigated the effect of Na-ion implantation on the corrosion resistance of titanium, the precipitation of calcium phosphate in a simulated body fluid (SBF) and the cytocompatibility of MG-63 cells. The Na-incorporation increased the corrosion resistance of cp titanium most likely due to the formation of amorphous layer on titanium. Furthermore, the Na-incorporated surface formed dense layers of the calcium phosphate, but non-incorporated titanium did not form a dense layer. However, the Na-incorporated and non-incorporated surfaces revealed negligible differences in the viability of the cells and their ability to spread on the investigated surfaces.

2 Aims

Study I: To investigate the surface chemistry and morphology of recently developed commercially available dental implants (TiUnite®, OsseoSpeed®, Osseotite®, and SLA®).

Study II: To investigate the effect of the MePIIID process parameters, i.e., plasma sources of magnesium and calcium, ion dose, and acceleration voltage on the surface chemistry and morphology of screw-type titanium implants.

Study III: To investigate the effects of surface chemistry and surface topography on the rate and strength of osseointegration.

Study IV: To investigate the effect of calcium concentration on the bone tissue response to Ca-incorporated titanium implants

Study V: To investigate the bone response to Mg-incorporated titanium oxide chemistry prepared with MePIIID process on titanium implants.

3 Materials and Methods

3.1 Commercially Available Dental Implants

Commercially available titanium implants, such as TiUnite® (3.75×7mm, Nobel Biocare, Göteborg, Sweden), OsseoSpeed® (4.00×11mm, Astra Tech AB, Mölndal, Sweden), SLA® (4.10×10mm, Institute Straumann, Waldenburg, Switzerland), and Osseotite® (3.75×8.5mm, Implant Innovation, FL, USA) were purchased from local distributors. These implants are fabricated with chemical etching or anodic oxidation processes. Two specimens for each type implant were analyzed

3.2 Design of Experimental Titanium Implants

Commercially pure titanium (grade 4) screw shaped implants were used in study II, III, IV and V. The implants used in animal experiments (study III, IV and V) have no cutting edge.

3.3 Sample Preparations

Surface chemistry modifications of the titanium implants in the present thesis were performed with PIIID and MAO processes. Table 1 summarized the implants group and their modification methods.

Table 1. Implant groups and their surface modification methods

Study	Implant group	Surface modification
Study II	EP	CNC machining + electropolishing
	IMg1, IMg2, IMg3, IMg4, IMg5	CNC machining + electropolishing + Mg PIIID
	ICa1, ICa2, ICa3	CNC machining + electropolishing + Ca PIIID
Study III (*in vivo*)	Turned implant	CNC machining
	Blasted implant	CNC machining + blasting with Al_2O_3 particles (75 μm)
	Mg implant	CNC machining + blasting with Al_2O_3 particles (75 μm) + MAO
Study IV (*in vivo*)	Ca4	CNC machining + MAO
	Ca6	CNC machining + blasting with TiO_2 particles (100-150 μm) + MAO
Study V (*in vivo*)	IO	CNC machining + O PIIID
	IMg	CNC machining + Mg PIIID

3.3.1 PIIID Process

MePIIID process was performed using metal arc plasma and negative high voltage pulse. The metal arc plasma was generated from metal load type Mg and Ca sources triggered by a pulse supply (100V), and then guided to titanium samples using a magnetic coil. The magnetic coil filters heavy particles produced from the plasma generation, thus enabling to guide pure plasma ions. When the guided metal arc plasma was arrived to the samples, the metal arch plasma was attracted and incorporated into titanium surfaces by the negative high voltage pulse (0-40kV). The signals used for triggering the metal arc plasma and the negative high voltages were synchronized to achieve successful ion incorporation. Fig. 2 illustrates a brief overview of the MePIIID process. O PIIID process was conducted using oxygen plasma and the negative high voltage pulse. The oxygen plasma was produced by a radio frequency generator at the oxygen pressure of 0.1 Pa. By synchronizing the RF generator and the negative high voltage source, the oxygen plasma ions were incorporated to titanium samples. The detailed sample preparations using the MePIIID and O PIIID processes in studies II and V were described below and summarized in Table 2.

i) **Study II**: Using metal arc plasma of Mg and Ca sources, the MePIIID process was performed to the electropolished titanium of screw-shape implants. The machined-turned surfaces were galvanostatically electropolished in a mixture of 3M surphuric acid and methanol at -7°.[103] Prior to the MePIIID process, the electropolished samples were degreased by ultra-sonication in an aqueous solution of phosphate-free Extran® MA 03 (Merck, Darmstadt, Germany)/deionized water (1:100) and absolute ethanol for 2 × 15 min. To generate the metal arc vacuum plasma, metal rod types of Mg and Ca were connected to arc-generator and triggered with 100V. Incident ion fluences per pulse were calculated by measuring current densities on titanium surfaces and by using the mean ion charges of Mg and Ca. The mean charge of metal arc plasma is 1.54 for Mg and 1.93 for Ca.[104] By controlling processing time and incident ion fluences, Mg and Ca ions were incorporated into titanium surfaces with three different ion doses (5×10^{15}, 10×10^{15}, 50×10^{15} ions/cm^2). The plasma ions were incorporated into titanium surfaces using three different negative voltage pulses (10kV, 13.6kV, 16.7kV). Totally eight types of samples were prepared with the MePIIID process (see Table 2)

ii) **Study V**: IMg and IO implants were prepared with the MePIIID and O PIIID processes, respectively (see Table 2). The MePIID and OPIIID processes were performed to machined-turned cp titanium. Using 20kV of the negative high voltage pulse, magnesium and oxygen plasma ions were incorporated into titanium surfaces at a dose level of 50×10^{15} ions/cm^2. To generate the magnesium arc plasma, metal rod types of Mg were connected to arc-generator and triggered with 100V. The oxygen plasma was generated by the RF generator at the oxygen pressure of 0.1 Pa.

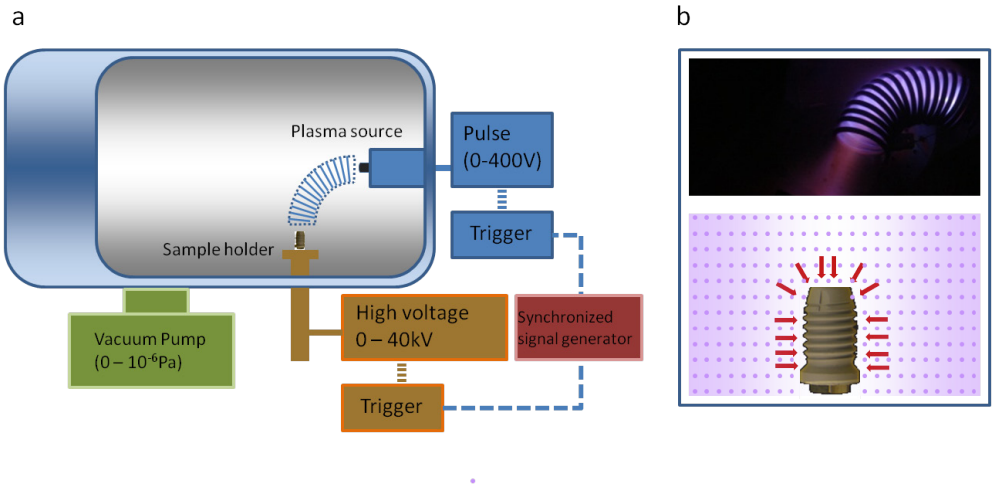

Fig. 2. Schematic illustrations of the MePIIID process: a) The metal plasma generated by a pulse supply (0-400V) was filtered and guided to the sample. A synchronized signal with the pulse generator triggered the negative high voltage pulse (0-40kV) connected to the samples, thus incorporating the plasma ions into the sample surface. b) The guided plasma ions perpendicularly incorporated into the samples surfaces, which enables to modify surface chemistry of the screw-shape implants having a complex geometry.

Table 2. Process parameters of the MePIIID and OPIIID used in studies II and V

Study	Sample	Plasma source	Incident ion dose (ions/Cm^2)	Acceleration voltage (KV)	Working pressure (Pa)	Surface type
Study II	IMg1	Mg	5×10^{15}	10	1.3×10^{-3}	Electropolished titanium
	IMg2	Mg	10×10^{15}	10	1.3×10^{-3}	
	IMg3	Mg	50×10^{15}	10	1.3×10^{-3}	
	IMg4	Mg	10×10^{15}	13.6	1.3×10^{-3}	
	IMg5	Mg	10×10^{15}	16.7	1.3×10^{-3}	
	ICa1	Ca	5×10^{15}	10	1.3×10^{-3}	
	ICa2	Ca	10×10^{15}	10	1.3×10^{-3}	
	ICa3	Ca	50×10^{15}	10	1.3×10^{-3}	
Study V	IO	O	50×10^{15}	20	1.3×10^{-3}	Machined turned titanium
	IMg	Mg	50×10^{15}	20	0.1Pa	

3.3.2 MAO Process

MAO process was conducted in galvanostatic mode using a Mg-containing electrolyte and a Ca-containing electrolyte, respectively. Currents and voltages were recorded continuously at 1-s intervals by an IBM computer interfaced with a DC power supply. The ripple variability was controlled to less than 0.1%. Two platinum plates having a surface area of 32 cm^2 were used as counter electrodes on both sides of the titanium anode. Fig. 3 illustrated the apparatus and cell of MAO process. The implants preparations using the MAO process were describe below:

i) **Study III**: Mg implants were machined turned, blasted with 75 μm particles of Al_2O_3, and then processed with the MAO using the Mg-containing electrolyte.

ii) **Study IV**: Two groups of Ca-incorporated titanium implants were prepared with the MAO process using the Ca-containing electrolyte. Ca 4.2% containing Ca4 implants were machined turned, and then processed by the MAO, while Ca 6.2% containing Ca6 implants were machined turned, blasted with TiO_2 particles (100-150 μm) and, finally processed by the MAO.

Prior to the MAO process, all the titanium samples were degreased by ultra-sonication in an aqueous solution of phosphate-free Extran® MA 03 (Merck, Darmstadt, Germany)/deionized water (1:100) and absolute ethanol for 2 × 15 min. After the MAO treatments, the samples were rinsed with absolute ethanol, and then dried in an oven at 60ºC over a day. Finally, the implants were sterilized in an autoclave prior to animal experiments.

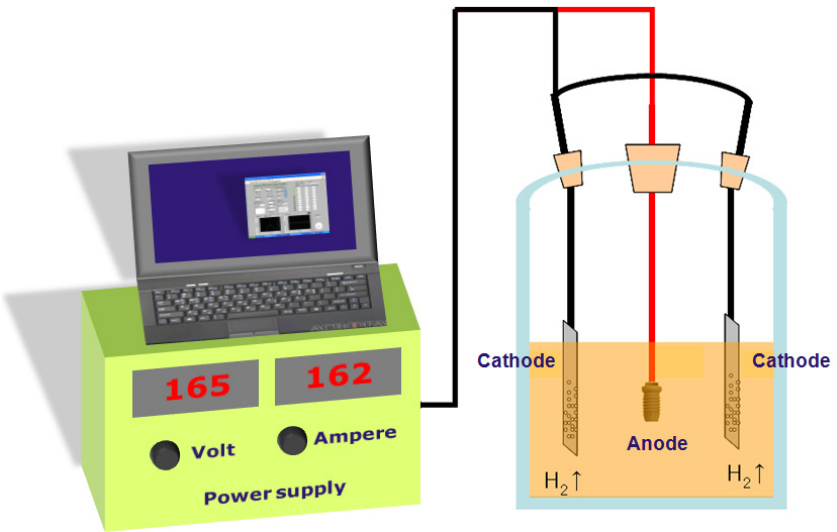

Fig. 3. Schematic illustrations of the apparatus and cell of the MAO process

3.4 Surface Characterization

3.4.1 X-ray Photoelectron Spectroscopy (XPS) Analysis

Surface chemistry of all the implants was analyzed by X-ray Photoelectron Spectroscopy (XPS, Sigma Probe, Thermo-VG, England). Monochromatic Al Kα (1486.7eV) X-ray was irradiated on the area of 400 μm between the second and third thread of the implants. The electron take-off angle was fixed at 45º and the vacuum pressure was below 10^{-9} torr during spectra data acquisition. Survey XPS data (widescan data) were acquired over 1200eV with pass energy of 50eV and a resolution of 1eV. XPS high resolution spectra were obtained at C 1s, Ti 2p, O 1s, Mg 2p, Ca 2p, P 2p, F 1s, Na 1s, Cl 2p, S 2p and Si 2p. The experimental conditions were over 15-20eV ranges, pass energy of 20eV and a resolution of 0.1eV. XPS data were acquired before and after sputtering for a better understanding of chemical bonding states between surface elements. Ar sputter cleaning was operated for 3 seconds (beam energy = 2keV, primary current = 2μA, rastered area 3.14mm^2). Relative atom concentration ratios were calculated based on the peak area and sensitivity factors of elements investigated. The binding energy of photoelectron was referenced to the C 1s line of adventitious hydrocarbon at 284.8eV. XPS spectra of Ti 2p, O 1s, C 1s, Mg 2p and Ca 2p were deconvoluted using a curve fitting program provided by a product company (Sigma Probe, Thermo-VG, England). Ti 2p spectra were deconvoluted to TiO_2, magnesium titanates, calcium titanates or titanium phosphates at ≈ 458.7 ± 0.2eV, Ti-OH at ≈ 457.9eV, Ti_2O_3 at 457.0eV ± 0.2eV, TiO at 455.3 ± 0.2eV and metal Ti at 453.8 ± 0.2eV. O 1s spectra were fitted with four sub-peaks, i.e., TiO_2, magnesium titanates, MgO or calcium titanates at 530.1 ± 0.2eV, titanium phosphates at 531.1eV ± 0.2eV, $(OH)_2$ or C-O at 531.7 ± 0.2eV, H_2O or C=O at 532.7 ± 0.2eV. Mg 2p spectra were resolved into two Gaussian sub-peaks, i.e., $Mg(OH)_2$ at 49.5eV and magnesium titanates or MgO at 50.3eV. Deconvolution data of Ca 2p were imposed to calcium titanates at ≈ 346.8eV and $Ca(OH)_2$ at ≈ 347.6eV.

3.4.2 Auger Electron Spectroscopy (AES) Analysis

Element depth profiles were measured by Auger Electron Spectroscopy (AES, Physical Electronics, model PHI 650). The electron beam with 2.5 μm × 4.0 μm probing area was accelerated at a 5KV of acceleration voltage and ≤ 10^{-9} torr. Continuous Ar etching was performed with sputtering energy of 2kV (etching rate: 3.7 nm/min) in study I and 0.5kV (etching rate: 0.5 nm/min) in study II and V.

3.4.3 Analysis of Surface Morphology and Pore Properties

Surface morphology of the titanium implants were analyzed by scanning electron microscopy (SEM, JEOL, LV-6380, Sweden). The SEM images were acquired with acceleration voltage of 20kV. The vacuum pressure was maintained below 1 × 10^{-5} torr. The load current (L.C) was approximately 85 μA. In order to reflect overall surface morphology, the SEM images were acquired at thread flanks of the implants except for SLA implant. The SEM images of SLA were

obtained from the thread valley. The magnifications of the SEM images were varied from × 3,000 to × 8,000 depending on the implant surfaces. From the SEM images, pore properties of the implants in study III and V were investigated using image measurement 2000 software (version 2.3, Tekno Optik AB, Skärholmen, Sweden).

3.4.4 Surface Roughness Measurement

Surface roughness of the screw-type implants were measured by an optical interferometer (MicroXam^{TM}, Phase shift, AZ, US). The interferometer has a lateral resolution of 110 nm and vertical resolution of 1 nm. The roughness was measured from three samples of each group at three thread-tops, thread-valleys, and three thread-flanks, totally 27 measurements per group. The measuring area was fixed to 230 × 230 μm^2 and the Gaussian filter (50 × 50 μm^2) was applied for removing the waviness and error forms. The evaluated roughness parameters were Sa (arithmetic average height deviation, μm) and Sdr (developed surface ratio, %).

3.5 Implant Insertion and Implant Group

Totally 29 of New-Zealand white rabbits were used in the present thesis: 10 for study III, 9 for study IV and 10 for study V. The mean weight of the rabbits at operation was 3.89kg for study III, 4.6kg for study IV and 4.3kg for study V. The animal experiments were approved by the local animal ethics committee at the Karolinska Institute, Stockholm, Sweden.

For surgery, the animals were anesthetized with intramuscular injections of fentanyl and fluanisone (Hypnorm Vet, Janssen, Saunderton, UK) at 0.5 ml/kg body weight and intraperitoneal injections of diazepam (Valium, Roche, France) at 2.5 mg/animal. Prior to surgery the shaved skin was carefully washed with a mixture of iodine and 70% ethanol. Local anesthesia with 1.0 ml of 5% Xylocaine (AstraZeneca, Södertälje, Sweden) was administered to the tuberositas region of the bone where the incision was planned, under aseptic conditions. The skin and fascial layers were opened and closed separately. The periosteal layer was gently pulled away from the surgical area and was not resutured. Totally 136 implants used in the thesis were inserted in tuberositas tibia region and were allowed to penetrate the first cortical region only. During all surgical drilling sequences low rotary drill speeds (not exceeding 2000 rpm) and saline cooling were used. The animals were kept in separate cages and immediately after surgery were allowed full weight-bearing. The animals were sacrificed by intravenous injections of Pentobarbital® (Apoteksbolaget, Uppsala, Sweden) at a given follow-up period. The implants groups were summarized in Table 3 and detailed insertion protocols were described below.

i) **Study III**: Three implants (n = 30), one of each group, were randomly placed in one tibia and, after 3 weeks, another 3 implants (n = 30, one of each group) were placed in the other tibia. The follow-up time was 6 weeks.

ii) **Study IV**: Two Ca4 implants (n = 18) were inserted in the tuberositas tibia region. In the corresponding site of the contra lateral leg, two Ca6 implants (n = 18) were inserted. The healing time was 6 weeks.

iii) **Study V**: Two Mg-incorporated implants (IMg, n = 20) were inserted in one side and two O-incorporated implants (IO, n = 20) were inserted in the other side. The follow-up time was 10 weeks.

Table 3. Implant groups of *in vivo* experiments

Study	Implant group	Number	Healing time	Surface chemistry
Study III	Turned implant	20	3 and 6 weeks	mainly Ti, O and C
	Blasted implant	20	3 and 6 weeks	mainly Ti, O, C and Al
	Mg implant	20	3 and 6 weeks	≤9.2% Mg, Ti, O and C
Study IV	Ca4	18	6 weeks	6.6% Ca, Ti, O and C
	Ca6	18	6 weeks	4.2% Ca, Ti, O and C
Study V	IO	20	10 weeks	mainly Ti, O and C
	IMg	20	10 weeks	9% Mg, Ti, O and C

3.6 Measurements of Bone Responses to Titanium Surfaces

3.6.1 Biomechanical Strength

3.6.1.1 Removal Torque (RTQ)

The strength of bone implant integration was evaluated by the removal torque (RTQ) test which measures the torque (force) needed to loosen the implant in the bone bed. This is a 3-dimensional biomechanical measurement roughly reflecting the interfacial shear strength between bone and implant.[105] The equipment consists of an electronic device incorporating a strain-gauged transducer, which enables controlled torque analysis of the peak loosening torque.[105] The peak removal torque was measured on the implants placed in the tibiae after 3, 6 and 10 weeks of healing.

3.6.1.2 Shear Strength

The shear strength, force per unit area (N/mm^2), was evaluated as following methods: $shear\ strenth = \frac{T}{\pi \times d \times l \times r}$, where T = removal torque in Nmm, d = mean diameter of the implant (3.45 mm), r = lever arm (= radius 1.725 mm), l = the bone length at the interfacial zone of bone and implant[106]. Four different bone lengths were used for shear strength calculations as follows:

Method A: measuring solid bone length from all threads of the unscrewed (RTQ tested) implants.

Method B: measuring solid bone length from three best consecutive threads in cortical region of the unscrewed implants.

Method C: measuring bone contact length from all threads of the non-unscrewed (non-RTQ tested) neighboring implants.

Method D: measuring bone contact length from three best consecutive threads in cortical region of the non-unscrewed neighboring implants.

The Fig 4 illustrates how to measure the solid bone length at the destroyed interface between bone and unscrewed-implants. In study IV, the shear strengths were calculated using method A, B, C and D, while method C was used in study V for the shear strength evaluation.

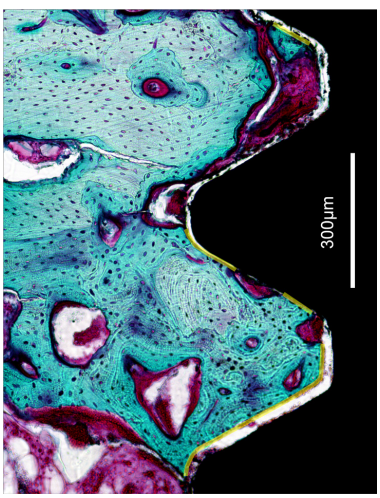

Fig. 4. Light micrograph of ground sections from the removal torque tested implants in bone, illustrating how to measure the solid bone length at the interfacial zone between bone and implant. The solid bone in the shear strength calculation is defined as the old cortical bone and newly formed bone except soft tissues. The solid bone length (yellow line) was measured along the destroyed interface between bone and implant.

3.6.1.3 Rate of Osseointegration

The rate of osseointegration was defined as the change in RTQ value over a particular healing time. The rate of osseointegration can be expressed as described in the following two cases[29]:

a) for the healing period from day 0 to the very first follow-up time:
Osseointegration rate = ΔRTQ / Δhealing time - α

b) for the healing period from the very first follow-up to the next follow-up:
Osseointegration rate = ΔRTQ / Δhealing time

The constant α is RTQ value at day 0 / the very first follow-up time. In study III, the constant α was presented as α_m, α_b and α_t for the Mg implants, blasted-implants and machined-turned implants, respectively.

3.6.2 Histomorphometry

3.6.2.1 Sample Preparation

The implants inserted into the distal part of the tibia in studies IV and V were prepared for undecalcified cut and ground sections using the Exakt cutting and grinding system.[105,107] The sections were ground to a final thickness of about 20 μm and stained with toluidine blue mixed with pyronin G.

The implants inserted into the proximal part of the tibia (removal torque tested implants) in study IV were prepared for cut and ground sections with the same procedures above. The sections were stained with basic fuchsin[10,108] and used only for the measurement of the solid bone length at the destroyed interface between bone and implant to calculate the shear strength.

3.6.2.2 Quantitative and Qualitative Analyses on the Stained Sections

The quantitative and qualitative observations of the stained sections were performed by a light microscope equipped with an image analysis software (Ecllips 80i, Tekno Optik AB, Skärholmen, Sweden). For histomorphometrical analyses, bone metal contact (BMC), bone area (BA) and newly formed bone were quantified. BMC and BA values were measured in all threads and three best consecutive threads in cortical region.[105] The newly formed bone were analyzed in two zones[12]: 1) inside the threads located in the old cortical region (zone A), 2) in the threads below the old cortex, i. e. the newly formed endosteal bone (zone B). In addition, new bone formation inside all threads (zone A and B) was quantified.

3.7 Statistical analysis

The data are presented as mean value ± standard deviation. Roughness comparisons of the experimental implants in study II and III were performed by analysis of variance (ANOVA): Post-Hoc multiple comparisons using SPSS 17 program, while the roughness values of implant surfaces in study IV and V were compared by the independent samples t-test. Bone responses to three groups in study III were compared by the multiple comparisons of Post-Hoc turkey methods whereas non-parametric Wilcoxon signed rank test were employed for the comparisons of biomechanical strengths and histomorphometrical data from the paired groups in study IV and V. The relationship between shear strengths calculated from different methods was assessed by Pearson correlation test using the same program.

4 Results

4.1 Surface Properties of Commercially Available Dental Implants

Fig. 5 showed SEM images of the clinical implants. The survey and high resolution XPS data were displayed in Fig. 6. Relative atom concentration and binding energies were summarized in Table 4. AES depth profiles of elements were demonstrated in Fig. 7.

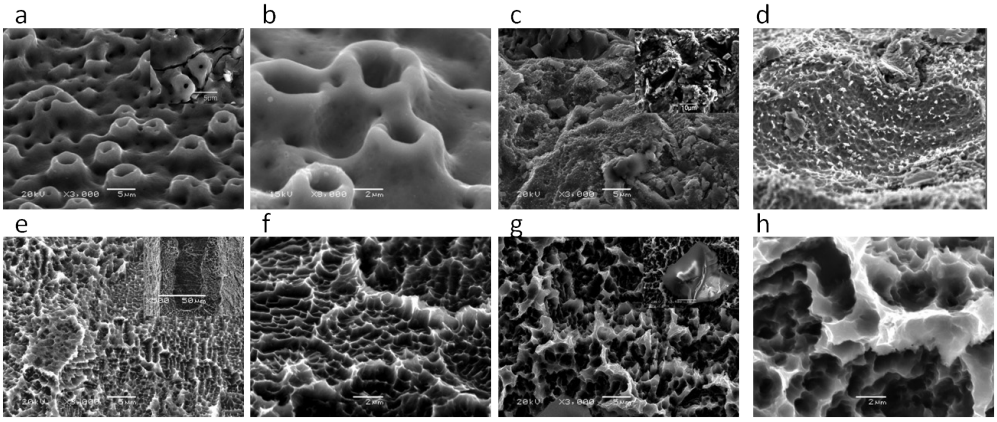

Fig. 5. SEM images of the TiUnite (a,b), OsseoSpeed (c-d),Osseotite (e-f) and SLA implants (g-h). The magnifications of ×3,000 and ×8,000 were used for SEM observation.

TiUnite: The TiUnite implants showed porous structure on the surface. The pore size was 0.5-3.0 μm, and sometimes elongated to ≈ 10 μm. The inset in Fig. 5a showed crack propagation on the TiUnite surface. Surface chemistry of the TiUnite was mainly composed of Ti, O, C and P. The atom concentration of P was ≈ 6.8% in XPS analysis. The peak binding energy of P 2p was 133.4eV, which indicated the presence of titanium phosphates. AES data confirmed the P-incorporation to the thick titanium oxide. Deconvoluted O1s data in Fig. 6d show significantly higher amount of (OH) on the TiUnite compared to the other implants.

OsseoSpeed: Surface topography of the OsseoSpeed implants were characterized with facets produced by blasting and fine etching pits. Sometimes, deep pits were observed on the surface. Surface chemistry of OsseoSpeed was mainly composed of Ti, O and C. The binding energy of Ti 2p and O 1s were congruent with the binding energy of Ti 2p and O 1s of cp titanium implants. F in the OsseoSpeed was barely detected at 0.3% in XPS analysis.

Osseotite & SLA: The acid-etched surfaces of the Osseotite and SLA implants similarly characterized by crystallographically oriented boundaries. However, the difference was a needle-like elevation structure with pore sizes of ≈ 1-2 μm for the Osseotite and a honey-comb structure of ≈ 1-3 μm for the SLA. The insets in Fig. 5 e and g showed some poorly etched area at a thread peak of the Osseotite and a remnant of blasting particle for the SLA, respectively. Main surface composition of the Osseotite and SLA was Ti, O and C. The binding energy of Ti 2p and O 1s were detected at ≈ 458.7eV and 530.1eV, respectively.

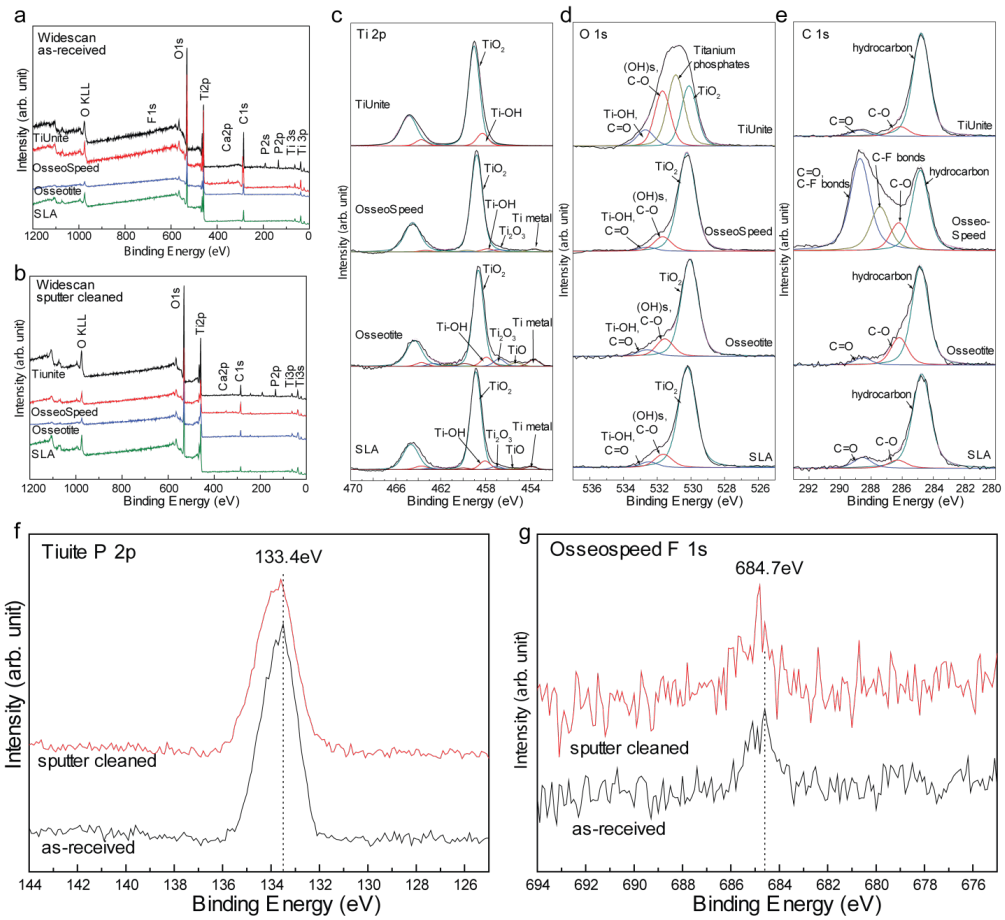

Fig. 6. The survey XPS data (a-b) and the high resolution XPS (c-g) data of four clinical implants: (a) XPS survey spectra of the as-received surfaces; (b) XPS survey spectra of the sputter cleaned surfaces; (c-e) Deconvoluted Ti 2p, O 1s and C 1s spectra of as-received surfaces; (f) P 2p in TiUnite; (g) F 2p in OsseoSpeed.

Table 4. Binding energies and atom concentration rate (at%) of elements at as-received and sputter-cleaned implants in XPS analysis

Elements	TiUnite				OsseoSpeed				Osseotite				SLA			
	AR*		SP**		AR		SP		AR		SP		AR		SP	
	at%	BE	at%	BE	at%	BE	at%	BE	at%	BE	at%	BE	at%	BE	at%	BE
Ti	12.0	459.0	17.5	459.2	11.8	458.8	20.7	458.8	16.7	458.6	30.9	458.7	20.1	458.7	29.5	458.7
O	45.2	530.7	55.1	530.9	33.1	530.1	39.6	530.3	38.7	530.0	48.4	530.4	47.1	530.1	55.9	530.4
P	6.8	133.4	9.5	133.5	-	-	-	-	-	-	-	-	-	-	-	-
F	-	-	-	-	0.3	684.7	0.4	684.8	-	-	-	-	-	-	-	-
C	35.1	284.8	17.0	284.8	53.2	284.8	38.2	284.8	44.0	284.8	20.8	284.8	32.0	284.8	13.9	284.8
N	1.0	400.5	0.9	400.6	0.3	400.5	-	-	0.6	400.5	-	-	1.0	400.6	0.8	400.5
Ca	-	-	-	-	1.3	350.8	1.1	347.5	-	-	-	-	-	-	-	-

AR*: As-received surface, SP**: Sputter-cleaned surface, at%: atomic concentration, BE: binding energy (eV).

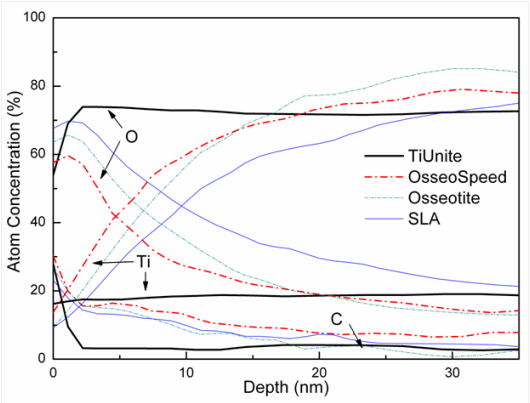

Fig. 7. The AES depth profiles with respect to the depth: Ti, O and C distribution of all the implants.

4.2 The Effect of MePIIID Process on the Surface Chemistry and Topography of Titanium

4.2.1 The Effect of Ion Source

Fig. 8 shows SEM images of the machined-turned, electropolished and MePIIID processed surfaces. These images demonstrate a characteristic feature of grooves and margins oriented during machine-turning procedures (Fig. 8 a) and leveled off by electropolishing, which resulted in mirror finish (Fig. 8 b). The Mg and Ca PIIID negligibly altered surface topography of the electropolished surfaces (Fig. 8 c and d). In addition, delaminations of deposited films or clusters of deposited particles were not observed at the implant surfaces after the MePIIID process. Surface roughness comparisons revealed that there were no significant differences in Sa and Sdr values at the thread top, valley and flank of the screw implants (Table 5).

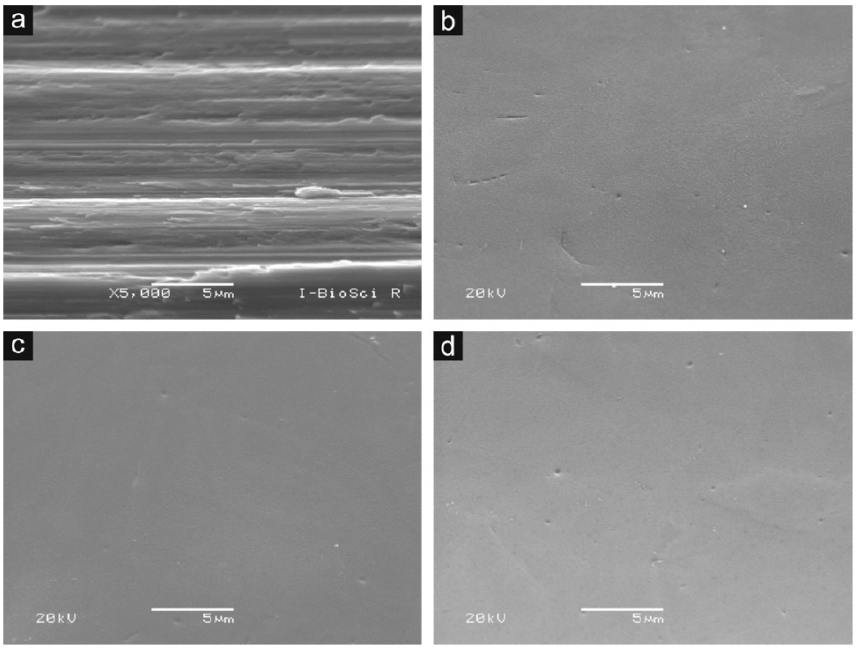

Fig. 8. The SEM images of (a) machined turned implant, (b) electropolished surfaces, (c) MgPIIID implant (IMg2) and (d) CaPIIID implant(ICa2)

Table 5. Surface roughness of Mg PIIID (IMg2), Ca PIIID(ICa2) and electropolished titanium implants (EP)

	Sa: mean (SD), μm				Sdr: mean (SD), %			
	Top	Valley	Flank	Total	Top	Valley	Flank	Total
IMg2	0.42 (0.03)	0.12 (0.02)	0.08 (0.02)	0.21 (0.16)	0.38 (0.21)	0.13 (0.07)	0.03 (0.02)	0.18 (0.18)
ICa2	0.39 (0.04)	0.10 (0.02)	0.06 (0.02)	0.19 (0.15)	0.42 (0.15)	0.09 (0.07)	0.02 (0.01)	0.17 (0.20)
EP	0.43 (0.03)	0.13 (0.02)	0.08 (0.02)	0.23 (0.15)	0.46 (0.13)	0.14 (0.29)	0.03 (0.01)	0.21 (0.20)

There were no significant differences in Sa and Sdr values among the samples at thread top, valley and flank, consequently showing no significant differences in total average values ($p>0.05$).

Survey XPS spectra in Fig. 9 demonstrate that the MePIIID process incorporated Mg or Ca ions into titanium. The major peaks were located at Ti 2p, O 1s, C 1s, Ca 2p and Mg 2p depending on the plasma source used. Sulfur was detected at the electropolished surface, but reduced to trace level after the MePIIID process. After Ar^{2+} sputter-cleaning, the peak intensities decreased at C 1s, but increased at Ti 2p, O 1s, Mg 2p and Ca 2p. Relative atom concentrations (at%) and binding energies of the elements are summarized in Table 6.

After the MePIIID process, Mg ions in Mg PIIID samples were detected in the range

values of 6% and 11%, while Ca ions in Ca PIIID samples were 5 to 8%. Ti amounts of the samples were decreased to more or less 3% after MePIIID.

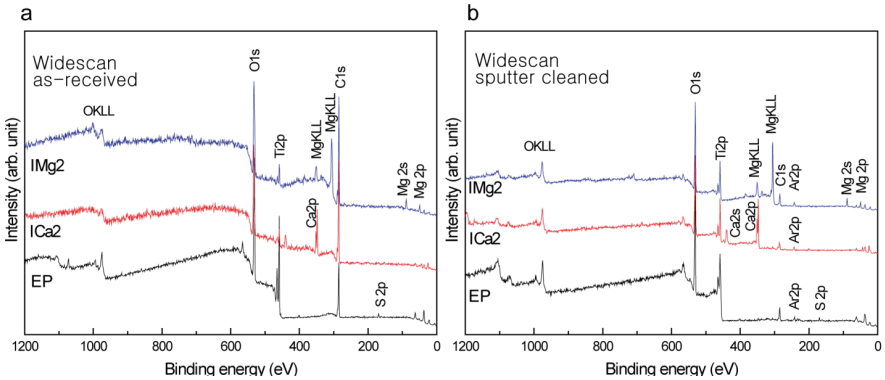

Fig. 9. XPS widescan of Mg PIIID (IMg2), Ca PIIID (ICa2) and electropolished (EP) samples: (a) XPS data of the as-received surfaces (b) XPS data of the sputter-cleaned surfaces.

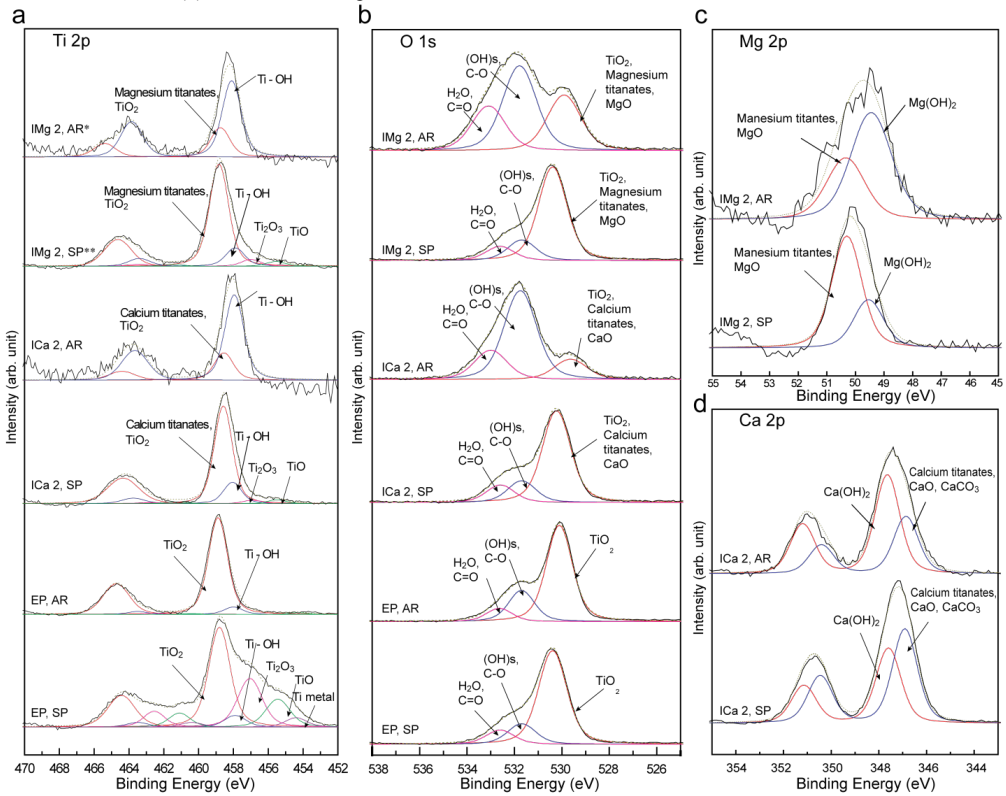

Fig. 10. XPS high resolution data of Mg PIIID (IMg2), Ca PIIID (ICa2) and electropolished (EP) implants on the as-received and sputter cleaned surfaces: (a) Ti 2p, (b) O 1s, (c) Mg 2p and (d) Ca 2p.

Table 6. Relative atom concentration rate (at.%) and binding energies of elements at as-received and sputter cleaned samples in XPS analysis

	Mg PIIID										Ca PIIID						Reference	
PIIID parameters																		
Plasma source	Mg arc plasma										Ca arc plasma						Electro-polished titanium screw	
Acceleration voltage	10KV				13.6KV		16.7KV				10KV							
Ion dose (ions/cm^2)	5×10^{15}		10×10^{15}		50×10^{15}		10×10^{15}		10×10^{15}		5×10^{15}		10×10^{15}		50×10^{15}			
Sample abbreviation	IMg1		IMg2		IMg3		IMg4		IMg5		ICa1		ICa2		ICa3		EP	
XPS Atom concentration rate (%)	AR*	SP**	AR	SP	AR	SP	AR	SP	AR	SP	AR	SP	AR	SP	AR	SP	AR	SP
Ti	2.3	11.9	2.1	9.7	2.0	8.1	2.2	10.8	3.6	12.3	2.1	11.0	2.0	8.9	1.3	3.2	13.2	32.6
O	35.9	63.9	35.4	66.8	39.0	64.4	31.4	65.3	42.8	68.7	28.8	57.1	27.0	57.5	35.9	60.1	39.4	58.7
C	53.5	7.9	52.8	6.4	47.3	7.2	58.0	7.9	47.0	6.7	64.6	17.5	64.3	17.2	55.2	18.1	44.8	7.2
Mg	8.1	16.3	9.5	17.1	11.0	20.3	8.2	16.0	6.6	12.3	-	-	-	-	-	-	-	-
Ca	-	-	-	-	-	-	-	-	-	-	5.3	14.5	6.3	16.4	7.6	18.7	-	-
S	-	-	0.2	-	0.7	-	0.2	-	-	-	0.2	-	0.4	-	-	-	1.2	1.5
N	0.2	-	-	-	-	-	-	-	-	-	-	-	-	-	-	-	1.4	-
XPS Peak binding energy (eV)	AR	SP	AR	SP	AR	SP	AR	SP	AR	SP	AR	SP	AR	SP	AR	SP	AR	SP
Ti2p3	458.2	458.8	458.2	458.7	458.2	458.8	458.4	458.8	458.5	458.8	458.0	458.6	458.0	458.5	457.1	457.8	458.8	458.8
O 1s	532.0	530.5	532.0	530.5	531.9	530.5	532.0	530.5	532.0	530.4	531.8	530.3	531.8	530.2	531.9	532.0	530.1	530.3
Mg2p	50.0	50.2	49.5	50.1	49.6	50.0	50.0	50.1	50.5	50.2	-	-	-	-	-	-	-	-
Ca2p3	-	-	-	-	-	-	-	-	-	-	347.4	347.2	347.4	347.2	347.4	347.3	-	-

AR*: as-received surface, SP**: sputter cleaned surface.

XPS high resolution data in Fig. 10 show the effect of the MePIIID on the binding energy shift in Ti 2p (≈ -Δ0.7) and O 1s (≈ +Δ1.3). The deconvoluted XPS data presented that the MePIIID process increased the peak intensity of (OH)s, H_2O and Ti-OH and resulted in significantly hydroxylation of Ca and Mg. After sputter cleaning, the intensity of (OH)s, H_2O and Ti-OH were abruptly decreased.

AES depth profiles in Fig. 11 showed intermixed layers of cathodic arc deposition and plasma ion implantation to titanium oxide. At a given MePIIID parameter, the Ca PIIID process formed a thicker intermixed layer than the Mg PIIID did.

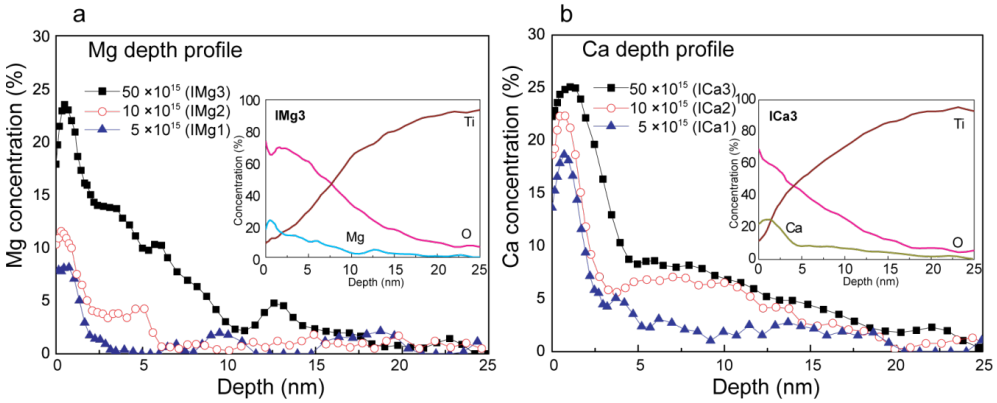

Fig. 11. AES depth profiles of Mg and Ca for three different ion doses: (a) Mg distribution; (b) Ca distribution. The inset spectra in (a) and (b) present the elemental distributions of Ti, O, Mg and Ca in IMg3 and ICa3 samples, respectively.

4.2.2 The Effect of Ion Dose

Fig. 12 displays the amount ratio of Mg/Ti and Ca/Ti in XPS analysis at the as-received and sputter-cleaned surfaces, respectively. The Mg/Ti and Ca/Ti increased with an increase of ion dose. At the acceleration voltage of 10kV, XPS data (Fig. 13) of the Mg PIIID samples showed no distinctive differences in Ti 2p, O 1s and Mg 2p irrespective of three ion doses, while XPS spectra of the Ca PIIID samples presented clear differences in Ti 2p and O 1s at the highest ion dose used. The AES depth profiles in Fig. 11 reveal that the signal intensity of Mg and Ca increase near surface with ion dose and the amount of plasma ion implanted deeper was increasing for higher ion doses at a given plasma source.

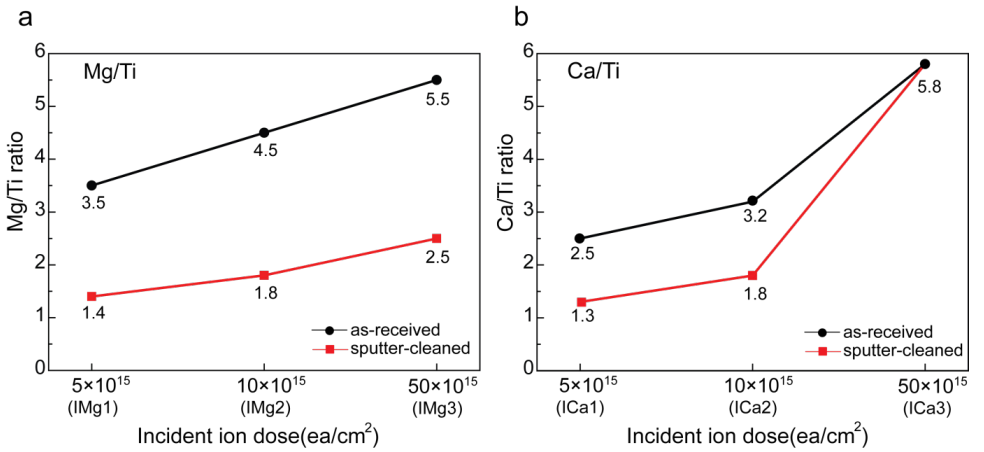

Fig. 12. The amount ratios of Mg/Ti and Ca/Ti in XPS analysis with respect to ion dose: (a) Mg/Ti of Mg PIIID samples; (b) Ca/Ti of Ca PIIID samples.

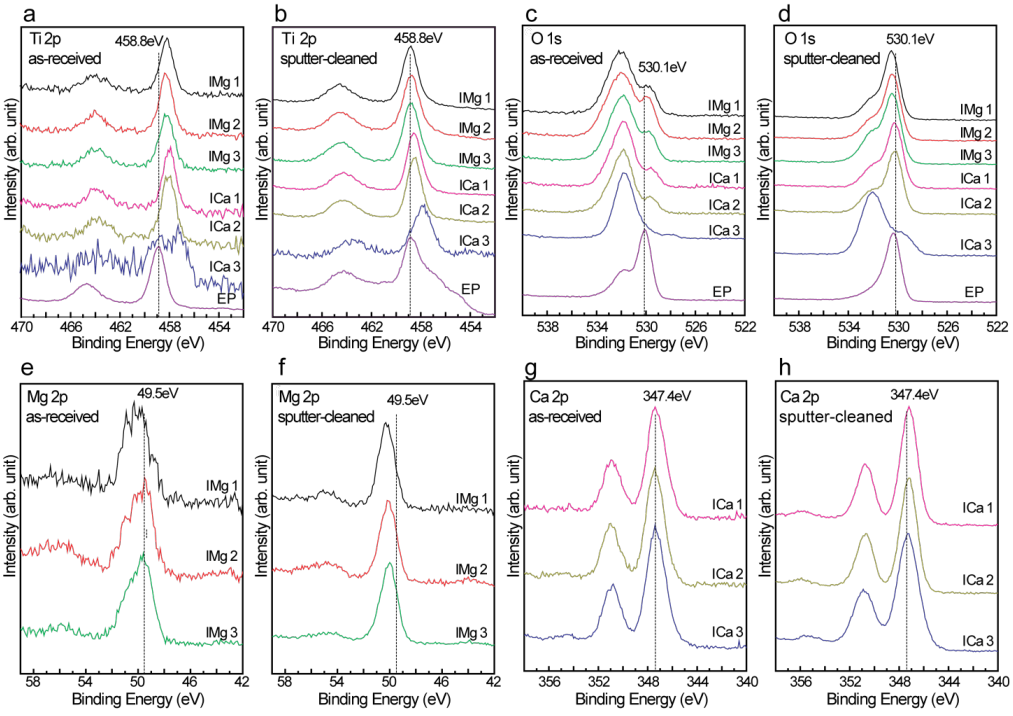

Fig. 13. High resolution spectra of the as-received and sputter cleaned implants for three different ion doses: Ti 2p (a-b), O 1s(c-d), Mg 2p (e-f) and Ca 2p (g-h)

4.2.3 The Effect of Acceleration Voltage

The amount ratio of Mg/Ti in XPS analysis (Fig. 14 a) decreased with acceleration voltage at an incident ion dose of 10×10^{15}. AES depth profile in Fig. 14 b revealed that the amount of Mg decreased with acceleration voltage near surface. The high resolution XPS spectra in Fig. 15 show peak binding energy of Mg 2p shifted from ≈ 49.5eV to ≈ 50.5eV with increasing the acceleration voltage.

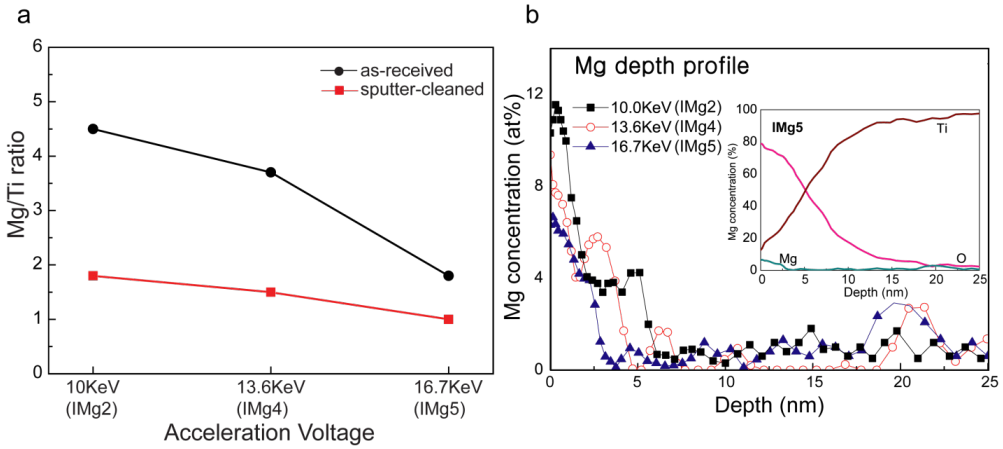

Fig. 14. The amount ratios of Mg/Ti in XPS analysis (a) and AES depth profiles of Mg (b) with respect to acceleration voltage. The inset spectra presented the distributions of Ti, O and Mg at the IMg5 implants.

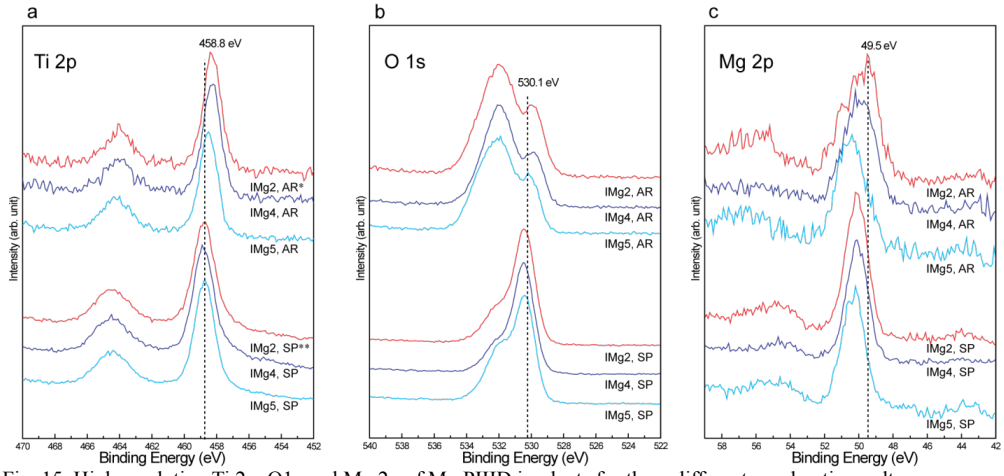

Fig. 15. High resolution Ti 2p, O1s and Mg 2p of Mg PIIID implants for three different acceleration voltages.

4.3 Surface Properties of Experimental Implants used in *in vivo* Studies

Surface topography of the experimental implants used in *in vivo* studies was displayed in Fig. 16. Roughness values of Sa and Sdr were shown in Table 7. Survey and high-resolution XPS of the implants were described in Fig. 17 and 18, respectively. Relative atom concentration rates and binding energies were summarized in Table 8.

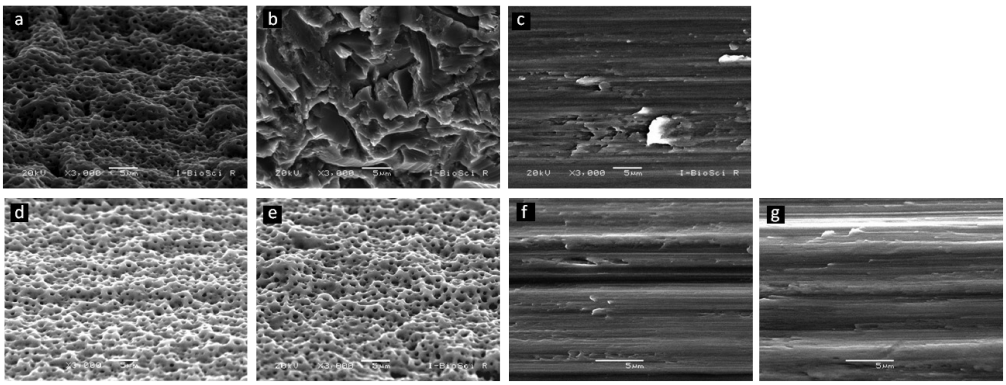

Fig. 16. The SEM images of the implants: (a) Mg implant; (b) blasted implant; (c) turned implant; (d) Ca4 implant; (e) Ca6 implant; (f) IO implant; (g) IMg implant

Study III: SEM images in Fig. 16 showed the microporous structures in the Mg implants (a), blasted pit structures in the blasted implants (b) and a feature of margin and grooves in the machined-turned implants (c). The Mg implants demonstrated a significantly lower Sa values than the blasted implants (0.69 ± 0.09 vs. 0.82 ± 0.09 µm, p = 0.007). Both of the Mg and blasted-implants revealed significantly higher Sa and Sdr values than the turned implant. Survey XPS data showed the characteristic elements of the implants, such as Mg for the Mg implants and Al for the blasted implants. The atom concentration of Mg ion was ≈ 6.2% for the as-received surface and ≈ 9.2% for the sputter-cleaned surface. The binding energy of Mg 2p was ≈ 50.5eV.

Study IV: Fig. 16 displayed the SEM images of the Ca4 (d) and Ca6 implants (e). The microporous structures were found on the implant surfaces. The mean porosity was 19.5 ± 3.3% for the Ca4 implants and 19.5 ± 3.9% for the Ca6 implants. The pore size varied from 0.2 to 1.5 µm for the Ca4 implants and from 0.3 to 1.5 µm for the Ca6 implants. The Ca6 implants showed significantly higher roughness values of Sa and Sdr than the Ca4 implants. Surface chemistry of the Ca4 and Ca6 implants were mainly composed of Ti, O, C and Ca. The Ca6 implants contained 6.6% of Ca and the Ca4 implants contained 4.2% of Ca. The peak binding energies of Ti 2p, O 1s and Ca 2p appear at ≈ 458.5eV, 530.0eV and 346.9eV, respectively (see Fig. 18). Deconvolution data revealed a similarity in the chemical bonding state of Ca in titanium oxides of the Ca4 and Ca6 implants.

Study V: Fig. 16 f and d presented the surface topography of the IO and the IMg implants, including a feature of machine-turning oriented grooves and margins. There were no significant differences in the surface roughness values of Sa and Sdr between the implants. The IMg and IO implants showed clear differences of surface chemistry: the IMg implants contained 9% of Mg, while the surface chemistry of the IO implants was mainly composed of Ti, O and C (see Fig. 17 and Table 8, below). The binding energy of Mg 2p was 49.8eV. XPS deconvolution data in Fig. 18 showed significant increase of hydroxyl group on the IMg and IO implants after PIIID process. AES data confirmed the Mg-incorporation to the titanium oxide of the IMg implants (data was shown in the manuscript of study V).

Table 7. Surface roughness of the implants used in the animal experiments (mean ± SD)

Study	Samples	Sa (μm)	Sdr (%)
Study III	Mg implant	0.69 ± 0.09	43.3 ± 19.4
	Blasted implant	0.82 ± 0.09	40.5 ± 7.9
	Turned implant	0.55 ± 0.28	10.6 ± 3.9
Study IV	Ca4	0.61 ± 0.17	9.15 ± 1.42
	Ca6	0.72 ± 0.17	13.0 ± 0.94
Study V	IO	0.52 ± 0.15	19.2 ± 18.1
	IMg	0.53 ± 0.18	17.8 ± 17.1

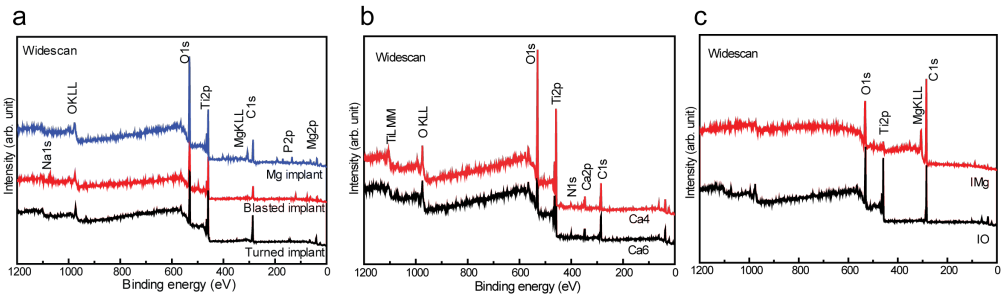

Fig. 17. XPS widescan of the implants: (a) Mg implant, blasted implant and turned implant in study III; (b) Ca4 and Ca6 implants in study IV; (c) IO and IMg implants in study V.

Table 8. Chemical compositions of the experimental implants used in the animal experiments (at. %)

Study	Sample	Ti	O	Mg	Ca	P	C	Al	trace elements
Study III	Mg implant	8.9	47.0	6.2	-	5.2	25.4	2.7	S, N, Ca, Na, Si
	Blasted implant	10.5	46.4	-	-	-	25.4	11.5	S, N, Ca, P, Na, Si
Study IV	Ca4	14.9	45.0	-	4.2	-	33.6	-	N,S, K, Si
	Ca6	15.4	46.9	-	6.6	-	29.1	-	N,S, K, Si
Study V	IO	11.1	37.7	-		-	49.9	-	N, Ca, Si
	IMg	3.6	34.4	9.0	-	-	52.6	-	N, Ca, Si

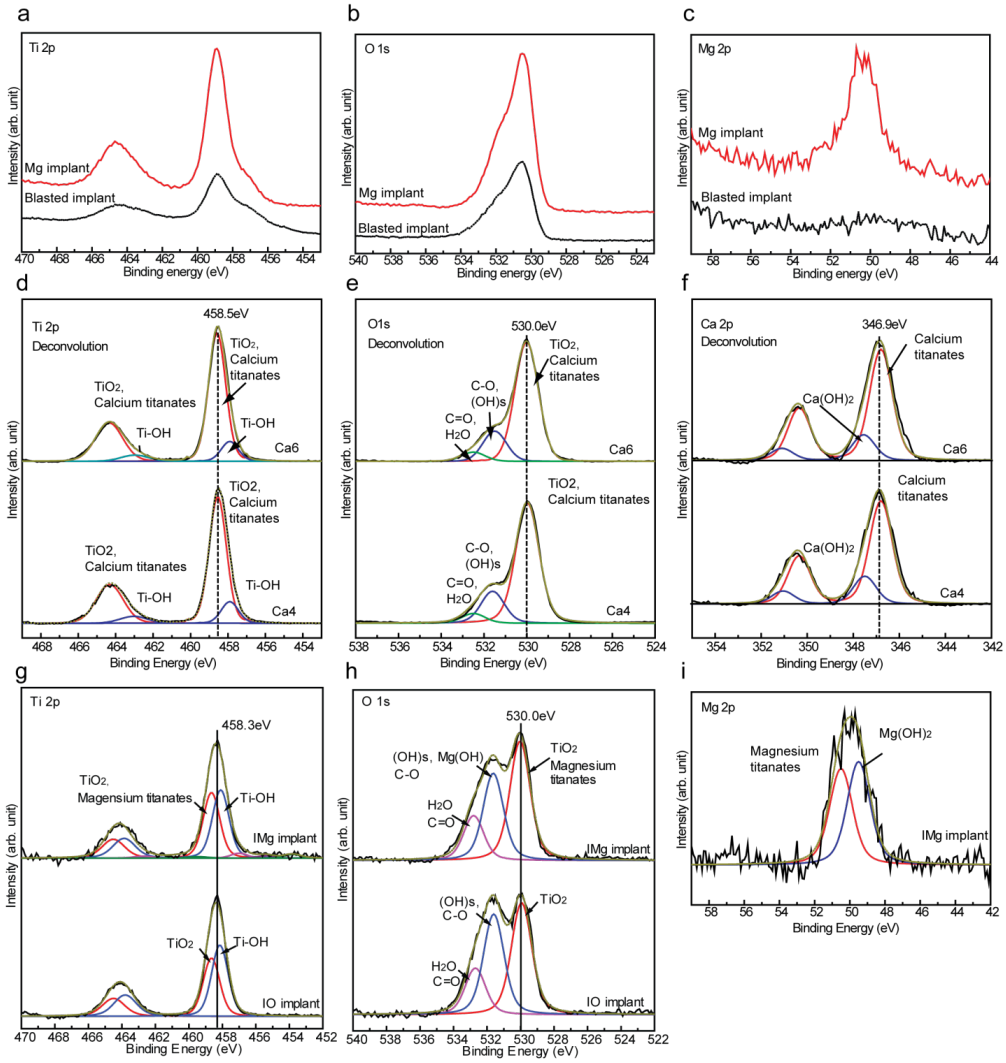

Fig. 18. The high resolution XPS data of the implants: (a-c) the Ti 2p, O1s and Mg 2p spectra of the Mg implant and blasted implant; (d-f) the Ti 2p, O 1s and Ca 2p spectra of the Ca4 and Ca6 implants; (g-i) the Ti 2p, O 1s and Mg 2p spectra of the IMg and IO implants.

4.4 Bone Responses

The bone responses of the implants in rabbit tibia were described at the following sub-sections. The osseointegration strengths of the implants in rabbit tibiae were measured with removal torque and summarized in Table 9.

Table 9. The osseointegration strength of the implants in terms of removal torque

Study	Group	Removal torque (Ncm)		
		3 weeks	6 weeks	10 weeks
Study III	Mg implant	25 ± 5*,**	39 ± 9*,**	
	Blasted implant	17 ± 4	30 ± 7***	
	turned implant	14 ± 3	20 ± 7	
Study IV	Ca4	-	32 ± 7	
	Ca6	-	30 ± 4	
Study V	IO	-	-	27 ± 3
	IMg	-	-	38 ± 3****

*: Significant difference ($p < 0.05$) between the Mg and turned implants

**: Significant difference ($p < 0.05$) between the Mg and blasted implants

***: Significant difference ($p < 0.05$) between the blasted and turned implants

****: Significant difference ($p < 0.05$) between the IMg and IO implants

4.4.1 Bone Responses in Study III

4.4.1.1 *In vivo* Removal Torque Test (RTQ)

At 3 weeks of healing, the Mg implants showed a significantly higher mean RTQ value than the turned implants (25.3 ± 4.7 vs. 13.5 ± 3.3 Ncm, n= 10, p = 0.0001) and the blasted implants (16.8 ± 3.6 Ncm, n = 10, p = 0.0001). There was no significant difference of mean RTQ values between the blasted and turned implants.

At 6 weeks of healing, the Mg implants demonstrated a significantly higher mean RTQ value than the turned implants (39 ± 8.5 vs. 19.6 ± 6.7 Ncm, n= 10, p = 0.0001) and the blasted implants (29.7± 6.5 Ncm, n = 10, p = 0.035). The blasted showed a significantly higher mean RTQ value than the turned implants (p = 0.0001).

4.4.1.2 Rate of Osseointegration

Fig 19 showed the rate of osseointegration at two different healing intervals. Between day 0 and 3 weeks, the Mg implants demonstrated significantly higher rate of osseointegration (Δ RTQ/ Δ weeks) than the blasted (p = 0.008) and turned implants (p = 0.004). As compared to the turned implant, Mg implants between 3 and 6 weeks demonstrated significantly rapid osseointegration (p = 0.039) while the blasted implants (p = 0.289) presented no significant

difference.

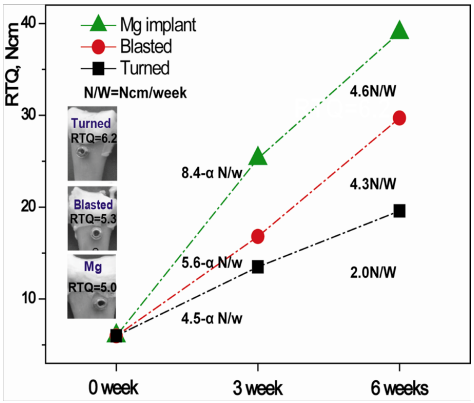

Fig. 19. The rates of osseointegration.

4.4.1.3 Ex vivo Removal Torque Test at day 0

The insets of Fig 19 showed Ex vivo baseline RTQ measurements of the implants in chicken tibia at day 0. The RTQ values of all implants were 6.2 ± 0.55 Ncm (range 6-7 Ncm, n = 8) for the turned implants, 5.3 ± 0.6 Ncm (range 5-6 Ncm, n = 8) for the blasted implants, and 5.0 ± 0.6 Ncm (range 5-6 Ncm, n = 8) for the Mg implants.

4.4.2 Bone Responses in Study IV

4.4.2.1 Removal Torque Test (RTQ)

The mean value of RTQ was 32 ± 7 Ncm for the Ca4 implants and 30 ± 4 Ncm for the Ca6 implants ($p = 0.37$). There was no significant difference between the two implants.

4.4.2.2 Shear Strength Comparison

The mean values and standard deviation of the shear strength are described in Table 10. The shear strengths revealed no significant differences between the Ca4 and Ca6 implants irrespective of the calculation methods ($p > 0.05$). Furthermore, at a given implant group, there are no significant differences of the shear strengths between the calculation methods using the unscrewed implants and the non-unscrewed neighboring implants ($p > 0.05$). The shear strength distributions in Fig 20 display that the shear strengths calculated from the unscrewed implants were more narrowly distributed than the shear strengths calculated from the non-unscrewed implants. There was strong correlation between the shear strengths estimated from two different threaded parts of implants, i.e., the all threads and the three best consecutive threads in cortical region: $r = 0.77$ ($p < 0.01$) for the methods using the unscrewed implants (Fig. 20 a) and $r = 0.97$ ($p < 0.01$) for the method using the non-unscrewed implants (Fig. 20 b).

Table 10. Shear strength calculations			mean ± SD
	Ca4	Ca6	p-values
Shear strength (N/mm^2)			
- method A: unscrewed implants, entire threads	16.7 ± 2.8	16.4 ± 2.5	0.59
- method B: unscrewed implants, 3 best consecutive threads	20.0 ± 4.1	19.6 ± 3.4	0.78
- method C: non-unscrewed implants, entire threads	19.6 ± 10.5	15.0 ± 5.9	0.14
- method D: non-unscrewed implants, 3 best consecutive threads	21.6 ± 9.3	17.7 ± 4.4	0.26

Note: Shear strength = $T/\pi drl$, where T = the removal torque, d = the mean diameter, r = the lever arm and l = bone length; (A) the solid bone length measured on the entire threaded part of the unscrewed implant; (B) the solid bone length measured on the three best consecutive threads in cortical region of the unscrewed implant; (C) the bone contact length measured on the entire threaded part of the non-unscrewed neighboring implant; (D) the bone contact length measured on the three best consecutive thread in cortical region of the non-unscrewed neighboring implant. The measurement of the solid bone length is illustrated in Fig. 4.

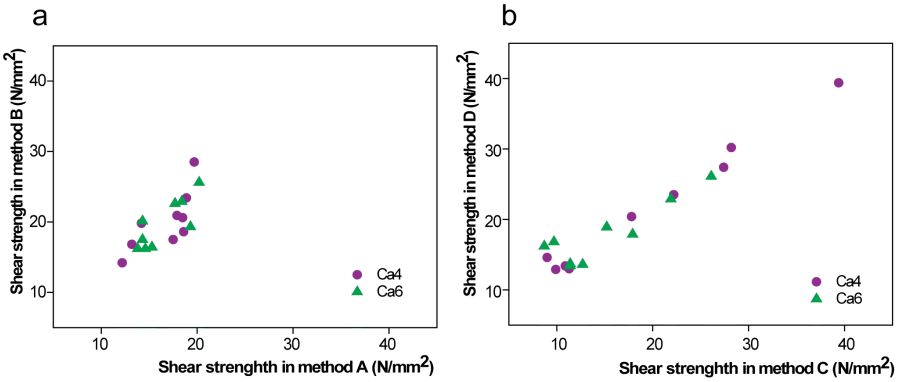

Fig. 20. The shear strength distributions: (a) the shear strength distribution calculated from the RTQ tested implants; (b) the shear strength distribution calculated from the non-RTQ tested neighboring implants.

4.4.2.3 Qualitative Light Microscopy Observations

Fig. 21 a and b show light microscopy observations of the undecalcified cut and ground sections from the non-unscrewed implants. Newly formed bone was clearly distinguished by the demarcation/cements line between dark and pale stained bone tissue. There were no distinct differences in apposition of new bone between the Ca4 and Ca6 implants. Inflammatory cells, such as macrophages and multinuclear giant cells, were observed in close vicinity of both implant surfaces. Fig. 21 c and d demonstrate the micrographs of the ground sections from the removal torque tested implants. Bone fractures and red blood cell infiltrations into the bone tissue were observed at both sections of the Ca4 and Ca6 implants.

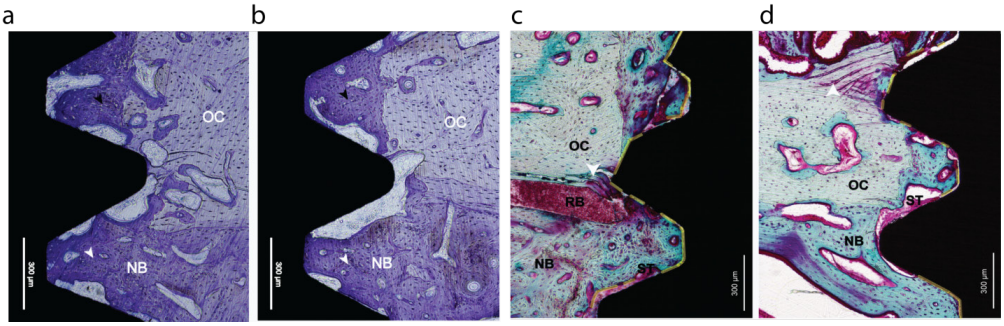

Fig. 21. Light microscopical observations on the undecalcified cut and ground sections in bone: Toluidine blue stained sections from non-RTQ tested implants (a: Ca4 implant, b:Ca6 implant) and basic-fuchsine-stained sections from the RTQ-tested implants (c: Ca4 implant, d:Ca6 implant). Newly formed bone (NB) including endosteal bone formation (black arrow head) and endosteal downgrowth (white arrow head) were clearly distinguished from old cortical bone (OC) by the demarcation line between dark and pale stained bone tissue both for the microphotograph of Ca4 implant (a) and Ca6 implant (b). Bone fractures (white arrow head) and blood cell infiltrations into the bone tissue were observed on the basic fuchsine stained sections (c-d) of the removal torque tested implants. The old cortical bone (OC; pale-green), the newly formed bone (NB; dark-green), red blood cell (RB; red) and soft tissue (ST; red and white) were clearly distinguished at the micrographs of Ca4 implant (c) and Ca6 implant (d). The length of solid bone (yellow line) was measured along the destroyed interface between bone and implant.

4.4.2.4 Histomorphometrical Measurements

Bone metal contact: The bone metal contact (BMC) measurements showed no significant differences between the Ca4 and Ca6 implants (Fig. 22 a). The mean value of BMC in all threads was 16.1 ± 6.7% for the Ca4 implants and 20.8 ± 6.8% for the Ca6 implants ($p = 0.18$). In the three best consecutive threads in the cortical region, the mean value of BMC was 34.5 ± 9.5% for the Ca4 implants and 40.6 ± 7.3% for the Ca6 implants ($p = 0.13$).

Bone Area: Bone area comparisons revealed no significant differences between the two implants (Fig. 22 b). The mean percentage of bone area inside all threads was 25.4 ± 8.7% for the Ca4 implants and 21.6 ± 7.1% for the Ca6 implants ($p = 0.26$). In the three best consecutive threads in the cortical region, the mean value of bone area was 52.5 ± 12.4% for the Ca4 implants and 46.5 ± 4.3% for the Ca6 implants ($p = 0.37$).

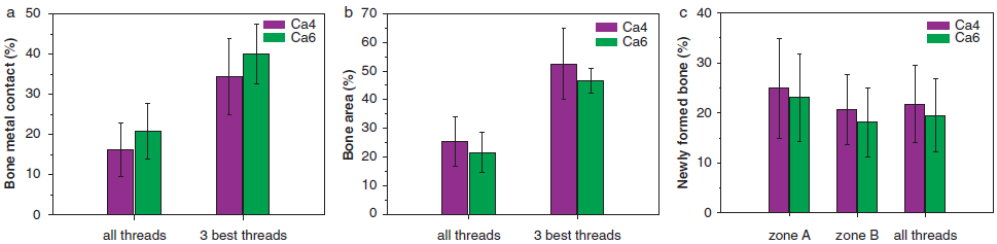

Fig. 22. The bone metal contact (a), bone area (b) and newly formed bone (c) of the Ca4 and Ca6 implants.

Newly formed bone: The amount of newly formed bone demonstrated no significant differences between the two implants (Fig. 22 c). The mean value of newly formed bone in zone A was 24.9 ± 7.1% for the Ca4 implants and 23.1 ± 8.7% for the Ca6 implants (p = 0.95), while the mean value in zone B was 20.6 ± 7.0% for the Ca4 implants and 18.1 ± 6.8% for the Ca6 implants (p = 0.95). The mean value of newly formed bone inside all threads was 21.8 ± 7.1% for the Ca4 implants and 19.5 ± 7.3% for the Ca6 implants (p = 0.37).

4.4.3 Bone Responses in Study V

4.4.3.1 Removal Torque Test (RTQ)

The mean value of RTQ was 27 ± 3 Ncm for the IO implants and 38 ± 3 Ncm for the IMg implants. The IMg implants showed significantly higher removal torque than the IO implants (p = 0.005).

4.4.3.2 Shear Strength Comparison

The mean value of shear strength was 15.0 ± 4.9 N/mm^2 for the IO implants and 18.1 ± 5.1 N/mm^2 for the IMg implants. The IMg implants showed significantly higher shear strength than IO implants (p = 0.011).

4.4.3.3 Histomorphometrical Measurements

Bone metal contact (BMC): The mean percentage of BMC is 26.1 ± 4.5% for the IO implants and 29.6 ± 5.9% for the IMg implants. The IMg implants showed significantly higher BMC% than the IO implants (p = 0.011).

Bone area: The mean value of bone area was 45.6 ± 6.3 % for the IO implants and 52.0 ± 3.4 % for the IMg implants. The IMg implants showed significantly higher bone area% than the IO implants (p = 0.038).

Newly formed bone: The mean percentage of newly formed bone was 42.7 ± 6.4 % for the IO implants and 49.3 ± 5.9 % for the IMg implants. The IMg implants demonstrated significantly higher newly formed bone% than the IO implants (p = 0.038).

5 Discussion

5.1 Discussion on Materials and Methods

5.1.1 Clinical Implants (Study I)

Surface chemistry and topography of the clinical implants were greatly dependent of treatment methods. The blasting and acid etching technique used for the Osseotite, OsseoSpeed and SLA implants resulted in mainly TiO_2, but rather changed surface topography. In contrast, electrochemical process for the TiUnite altered not only surface chemistry, but also created porous structures on surface.

The surface chemistry of the Osseotite, OssoSpeed and SLA was mainly composed of Ti, O and C. The Ti metal peaks of the Osseotite, OssoSpeed and SLA indicated that they have a thin oxide layer. However, XPS and AES data of the TiUnite implants showed P-incorporation into the thick titanium oxide. The binding energy of P, Ti and O may indicate the presence of titanium phosphates. In addition, TiUnite implants showed a higher amount of hydrated water (Ti-OH) and hydroxides (OH) on the surface as compared to the Ossotite, OsseoSpeed and SLA.

The surface topography of the TiUnite was characterized as a porous structure with a lot of craters while the other implants contained the etching pits and facets. Fine differences of the pits and facets were obvious between the OsseoSpeed, Osseotite and SLA implants due to differences of used blasting and etching parameters. Blasting particles were detected in the SLA implants. These particles deemed to be alumina residuals.[46]

5.1.2 Surface Modification Techniques

5.1.2.1 MePIIID and O PIIID Processes (Studies II and V)

In the present project, we employed the MePIIID technique to investigate the effect of the MePIIID on the surface chemistry and morphology of titanium oxide depending on the MePIIID parameter used and to produce ‘bioactive’ titanium including Mg and Ca ions on the titanium surfaces. It is a great advantage that the MePIIID process can alter surface chemistry of titanium oxide with negligible change of surface roughness by tailoring the plasma source, ion dose and acceleration voltage.[31,109] Furthermore, the cyclic process of repeating cathodic arc deposition and plasma immersion ion implantation formed the intermixed layer between the substrate and film[64,66], which prevents a possible delamination and bio-degradation of the MePIIID-treated

surface when exposed to biological environments.[38,70]

The MePIIID process produced the Mg- and Ca-incorporated titanium surfaces which chemical bonding states were mainly magnesium titanates and calcium titanates, respectively. The atom concentrations of plasma ions increased with ion dose and decreased with acceleration voltages. By tailoring the MePIIID parameters, such as plasma source, ion dose and acceleration voltages, we have successfully produced magnesium titanates surfaces containing ≈ 9% of Mg, which concentration is corresponding to the optimal Mg concentration of titanium oxide in a previous study.[81] Furthermore, titanium surfaces demonstrated a significant increase of hydroxyl groups on the surfaces after the MePIIID process. Due to the significant hydroxylation of titanium oxide after the MePIIID, the Mg- and Ca-incorporated titanium showed chemical shifts in Ti 2p and O 1s as compared to the non-treated titanium oxide.

The OPIIID process produced the O-incorporated titanium which was mainly composed of Ti, O and C. Similarly to the MePIIID process, the OPIIID treated titanium demonstrated a significant increase of hydroxyl group in Ti 2p and O 1s.

The IMg and IO implants prepared with PIIID process in study V demonstrated clear differences in surface chemistry: the IMg implants contained ≈ 9% of Mg in titanium oxide, while the IO implants were mainly composed of Ti, O and C. However, the two implants revealed no significant differences in surface topography as evaluated from roughness comparisons as well as SEM observations. From the surface analyses, it is certain that the PIIID process provides proper test and control groups for the investigation of the effect of Mg ions on the bone response.

5.1.2.2 MAO Process (Studies III and IV)

The MAO process not only incorporated Ca and Mg ions into titanium surfaces, but also created microporous structures in titanium oxide.[10,11,32] By controlling the MAO process parameters, we produced Ca-incorporated implants containing two different concentrations of Ca, but having similar chemical bonding states of Ca in titanium oxides. The chemical bonding states of Ca were mainly calcium titanates including small amounts of $Ca(OH)_2$. In case of the Mg-incorporated titanium, the chemical bonding states of Mg were mainly magnesium titanates. Surface roughness of Sa values were ranged from 0.61 to 0.72 μm after the MAO process. The Sa value of the titanium implants prepared with the MAO on the blasted surfaces were higher than the Sa values of the implants prepared with the MAO on the machined-turned surfaces.

5.1.3 Surface Characterization

5.1.3.1 XPS Analysis

XPS enables to investigate the chemistry of the outmost surface due to the short penetration depth of X-ray and the short mean free path (escape depth) of photoelectron.[77] In general, XPS data of as-received surfaces show the contaminants of C species, physically and chemically absorbed water, as well as main components of implant surfaces, such as Ti, O, Mg

and Ca. Therefore, it is necessary for us to compare XPS data from as-received and sputter-cleaned surfaces for a better understanding of surface components and their chemical bonding states. By comparing XPS data from as-received and sputter-cleaned surfaces, we found that more than 20% of carbon contaminates were present on the commercially available dental implants. Furthermore, the increase of Mg and Ca concentration after sputter cleaning indicated that Mg and Ca ion were incorporated into titanium surfaces after the MePIIID and MAO processes. Abrupt decrease of hydroxyl groups and the binding energy shift of Ti 2p after sputter cleaning revealed the significant hydroxylation of the MePIIID treated samples after exposure to air.

5.1.3.2 AES Analysis

AES analysis enables investigation of the chemical compositions of the implants and depth profiles of surface elements, such as Mg and Ca. However, the chemical compositions of the implants measured by AES were differed from the chemical compositions measured by XPS. This may be due to the difference in sensitivity factor to elements of XPS and AES.[75]

5.1.3.3. Interferometry

Surface roughness measurements presented the difference in surface topography of the implants depending on the surface treatment used. The Sa value was ≈ 0.21 μm for the implants prepared with the electropolishing/electropolishing + MePIIID process, ≈ 0.53μm for the implants produced with the CNC machining/ CNC machining + PIIID process, ≈ 0.82 μm for the implants prepared with the Al_2O_3-blasting process, ≈ 0.61μm for the CNC machining + MAO processes and ≈ 0.71μm for the TiO_2-blasting + MAO processes. The roughness measurements for the electropolished implants revealed a big difference of Sa values depending on the measuring site of the screw-shaped implants: the mean Sa value from the thread top was about 5.2 times higher than the mean Sa value from the thread flank.

5.1.4 Evaluation Methods for the Bone Responses to the Implants

5.1.4.1 Removal Torque Measurements and the Rate of Osseointegration

The strength and rate of osseointegration in the present thesis were evaluated on the basis of biomechanical measurements of removal torque.[105] The terminology of osseointegration strength reflects the bone integration to implants. Indeed, the strength and rate of osseointegration are valuable parameters to estimate how rapidly and strongly the implants integrate in bone during a given heal time.[12,29]

The rate of osseointegration in study III was calculated from the removal torque values after 3 weeks and 6 weeks of healing time. For the calculation of the osseointegration rate from day 0 to 3 weeks, the following equation have been used: (RTQ at 3 weeks) / (3 weeks) - α,

where α = RTQ value at day 0 / 3 weeks. The virtual mean RTQ values at the day 0 will be determined primarily by frictional force originated from compressive strength exerted upon implant insertion. Thus, all the groups in study III were supposed to share similar values of friction force and the constant α since all the implants had the same macroscopic geometry, and were inserted by a same surgeon according to the same surgical protocol. The ex-vivo experiments supported the validity of the hypothesis in that the differences of RTQ values were more or less 1 Ncm between the implant groups. The constant α has no influence on the p values.

5.1.4.2 Shear Strength Calculation

The shear strength in the present thesis was calculated by the simple formula based on the RTQ value and the bone length. For a 'proper' shear strength calculation, the shear strength as well as the bony contact length to implant surface need to be measured on the same implants. However, the interface between bone and implant was destroyed after removal torque testing, which makes it difficult to measure the direct bone contact length of the same implant. Thus, we approximated the bone contact length to unscrewed implants by using two methods in study IV: 1) measuring the solid bone length at the destroyed interface between bone and unscrewed implants and 2) measuring the bone contact length on non-unscrewed neighboring implants. Irrespective of the implant group in study IV (Ca4 and Ca6), the shear strength comparison revealed no significant difference between the methods using unscrewed and non-unscrewed implants. However, the shear strength converted from the unscrewed implants presented a more narrow distribution than the shear strength converted from the non-unscrewed implants. In study IV, the shear strength was calculated from two different threaded parts of the implants, such as the entire threads (all threads) and three best consecutive threads in cortical region. The correlation test revealed the strong correlation between the shear strengths converted from the entire threads and converted from three best consecutive threads. This strong correlation implies that the bone contact length to three best consecutive threads in the cortical region may be the determinant part of the total bone contact length for the shear strength calculation.

5.1.4.3 Histomorphometry

Undecalcified cut and ground sections with implant were stained with toluidine blue mixed with pyronin G for non-RTQ tested implants and stained with basic fuchsin for the RTQ-tested implants. The toluidine blue staining distinguished newly formed bone from the old cortical bone, while the basic fuchsin staining clearly presented the bone fractures and the infiltrations of red blood cell into bone tissue after the RTQ tests. Bone metal contact, bone area and newly formed bone were measured using the toluidine blue-stained sections.

5.2 Discussion on Results

5.2.1 Study III

At the healing time 3 weeks and 6 weeks, the Mg implants demonstrated significantly higher osseointegration strength than the turned and blasted implants. There was no significant difference in osseointegration strengths between the turned and blasted implants at 3 weeks of healing. However, the blasted implants significantly increased the osseointegration strength at 6 weeks of healing time, which can be explained with the significantly higher roughness of the blasted implants than the turned implants. According to previous studies, the blasted surfaces increased the bone integration strength with increase of Sa value in the range ≈ 0.4 to 2 μm.[13,14,110] In contrast, the Mg implants revealed significantly higher osseointegration strength than the blasted implants despite their significantly lower Sa values. This is most likely due to surface chemistry effect on the bone implant integration.[12,111] According to our previous studies[12,32,81,82], the bioactive surface chemistry of Mg implants strongly and rapidly increased the osseointegration. A number of experimental and clinical data provided evidences for the significant effect of surface chemistry modifications of titanium implants in osseointegration.[7,15,99,112-114]

The Mg implants showed a highly significant increase in the rate of osseointegration compared to the turned and blasted implants between day 0 and 3 weeks. Between 3 weeks and 6 weeks, the Mg implants demonstrated a highly significant increased osseointegration rate compared with the turned implants, but not the blasted implants. The difference of the osseointegration rate between two healing interval is 3.8 - α_m Ncm/week for the Mg implants, 1.3 - α_b Ncm/week for the blasted implants and 2.5 - α_t Ncm/week for the turned implants. These features represent three characteristic modes of osseointegration behavior: (i) the Mg implants had continuously increased the osseointegration strength up to 6 weeks; (ii) the blasted implants had increased osseointegration strength for the second 3 weeks compared with the first 3 weeks; (iii) the turned implants had increased the osseointegration strength for the first 3 weeks compared with the second 3 weeks.[29]

From this study, it is found that the Mg-incorporated titanium oxide enhanced the osseointegration in terms of bonding strength and speed. These results provide evidence for the surface chemistry-mediated osseointegration mechanism proposed by Sul[71], which facilitates rapid and strong integration of implants in bone, particular at earlier healing periods.

5.2.2 Study IV

The study IV investigated the effect of Ca ion concentration on the bone response to Ca-incorporated titanium. The Ca-incorporated implants prepared by the MAO process showed two different concentrations of Ca (4.2% and 6.6%), but revealed similar chemical bonding states of Ca in titanium oxide. The chemical bonding states of Ca in titanium oxide were mainly calcium titanates including small amounts of $Ca(OH)_2$. The overall bone response to the two investigated

titanium implants demonstrated no significant differences in RTQ, BMC, BA, newly formed bone and shear strength analyses irrespective of calcium concentration. In addition, LM observation revealed no significant differences in the bone apposition, the old and new bone area between the two tested implants. However, the results of the present thesis stand in clear contrast to the results in our previous studies where the osseointegration strength was measured by RTQ for two other types of Ca-incorporated implants. In the previous studies, the Ca 7%-containing implants revealed an increased RTQ value of 314% compared to pure machined-turned titanium, while the Ca 11%-containing implants showed an increased RTQ value of 153% compared to same types of cp titanium implants.[9,11] The discrepancy between the present and previous results may be explained by the similarities and differences in the chemical bonding states of Ca at the titanium implant surfaces: the similar chemical bonding state of Ca in the two implants used in the present thesis lead to no significant difference in the bone response whereas a two-fold difference in the increased rate of RTQ values resulted from the different chemical bonding state of Ca in Ca-incorporated implants of the previous studies. The two implants of the previous studies demonstrated clear differences in chemical bonding states of Ca: the peak binding energy of Ca2p was detected ≈ 347.3 for the Ca7%-containing implants and ≈ 347.8eV for the Ca11% implants.[9,11]

Ca-incorporated implants have shown improved bone responses in several *in vivo* studies. Although the action mechanism is not clearly understood underlying the previous findings, Ca ions in titanium play an important role on the enhanced bone tissue/cell integration to the implant surfaces via "electrostatic/ionic bonding" with adhesive proteins, i.e. proteoglycans, collagen, thrombospondin, fibronetin, vitronection, fibrillin, osteoadherin, osteopontin and bone sialoprotein. These polyanionic proteins can stimulate Arg-Gly-Asp (RGD) sequence and also trigger further recruitment of osteoprogenitor cells and osteoblasts via the Ca-signalling pathway.[11,33-35] The main driving force of this mechanism may be the movement of Ca ions from the Ca-incorporated implants. In general, an important factor affecting ion release from the oxidized surface of metals is the chemical bonding state of the metal oxide.[115] This indeed supports the explanation that the similar bone responses to the Ca-incorporated implants used in this project resulted from the similarity in chemical bonding state of Ca in titanium oxide.

Significantly different surface roughness of the two tested implants may, at least in part, have an influence on the bone response to titanium surface. Regarding the effect of surface roughness of the magnitudes cited, it has been reported that 'rough' implant surfaces enhance osseointegration compared to smoother surfaces.[3,14,116,117]. However, in the present thesis, somewhat rougher Ca6 implants revealed no significant difference in the osseointegration compared to smoother Ca4 implants, but differences in roughness were small, if significant. Perhaps this difference is compensated by the osteoconductive properties of Ca ion.

In the present thesis, mean shear strength of Ca-incorporated implants after 6 weeks of healing was 16.9 N/mm^2. This value is greater than the shear strength of machined-turned implants (14.8 N/mm^2) inserted into rabbit tibiae during 12 weeks. Probably, the Ca ions in titanium implants facilitate the rapid and strong integration of implants in bone.

5.2.3 Study V

The IMg implants showed significantly higher osseointegration strength than the IO implants after 10 weeks of healing. Furthermore, the IMg implants presented significantly higher percentages of BMC, BA, and newly formed bone than the IO implants. In shear strength comparison, the IMg implants demonstrated significantly higher strength than the IO implants. These results support the significant effect of Mg-incorporated titanium oxide chemistry on the bone integration to titanium.[12,32]

According to previous studies, bioactive surface chemistry including Mg, Ca, S and P ions reinforced the bone integration to titanium surfaces in terms of bonding strength and speed.[9,11,12,29] In particular, Mg-incorporated titanium oxide chemistry demonstrated significantly higher strength of osseointegration compared with experimental and clinical implants.[12,32] Based on the hypothesis of chemistry-medicated osseointegration mechanism, Sul et al explained that the Mg-incorporated titanium oxide chemistry facilitates the rapid and strong osseointegration, particularly at the early healing time.[12,29] In this study, the Mg-incorporated titanium oxide chemistry was produced by the MePIIID process. This process allows surface chemistry modification with negligible alternation of surface topography at the nanometer level thus enabling the investigation of the effect of bioactive surface chemistry on the osseointegration.[64,109] Indeed, surface properties of the IMg and IO implants demonstrated clear difference of surface chemistry, but showed negligible differences in their topography. Thus, the results of bone responses to the IMg and IO implants not only enabled to investigate “pure” contribution of Mg-incorporated titanium oxide chemistry on the osseointegration, but also provide strong evidence of the chemistry mediated-osseointegration mechanism.

6 Conclusions

1. Surface chemistry of commercially available dental implants is determined by experimental parameters of surface engineering techniques in use. The blasting and acid etching techniques generally do not change the surface elements of the titanium, consisting mainly TiO_2, but rather alter the surface morphology. In contrast, the electrochemical oxidation process not only changes surface chemistry due to incorporation of anions from the used electrolytes, but also produces microporous surface

2. The MePIIID technique modifies surface chemistry by tailoring plasma source with negligible alternation of surface topography at the nanometer scale, thus enabling the investigation of the effects of bioactive implant surface chemistry on the bone response.

3. The Mg-incorporated titanium prepared with the MAO process demonstrated significantly stronger osseointegration and most rapid osseointegration compared with the turned or blasted implants.

4. From the biomechanical and histomorphometrical measurements, the Ca-concentration difference of titanium surfaces had no significant influence on the bone response. This similar bone response in rabbit tibiae may be explained by the similarity of the qualitative Ca chemistry in titanium surfaces.

5. The Mg-incorporated titanium prepared by the MePIIID process demonstrated the significantly enhanced bone responses compared to the O-incorporated titanium. The results indicated that the Mg-incorporated titanium oxide chemistry most likely contributed to the enhanced bone responses to the implant surfaces.

7 Acknowledgement

I would like to thank all of you who have helped me with this thesis:

Associate professor Young-Taeg Sul for your never failing encouragement, patient, trust, support, critical discussion, and supervising throughout all this work. Without your enthusiasm and great knowledge on implant surfaces, this thesis would not exist

Professor Tomas Albrektsson for accepting my challenges on this work and for giving me wise comments and discussion

Professor Carina Johansson for your never failing encouragement, great discussion and teaching me histology

Professor Se-Jung Oh for your encouragement, support, expertise and collaborations

Hyun-Joo Lee for your endless help and support in XPS and XRD experiments

Dr. Youngsoo Jeong, Dr. Eungsun Byon, Dr Jong-Kuk Kim for your collaborations in surface modifications of titanium implants

Suyeon Cho for collaborations in XPS experiments

Petra Johansson, Maria Hoffman and Ann Albrektsson for your contribution in this work and your technical assistance at laboratory

All members of the department of Biomaterials in University of Gothenburg for your encouragement and scientific discussion

Jeong-Im Kang, Youngsoon Um, Ingemar Johansson for your great love, support, care and energy to me

My friends: Sang-Wook Lee, Goo-Hwan Jeong, Youngwoo Nam, Seon Namgung, Tae-Hoon Han, Hyuk-Jang Kwon, Hyeon-Chul Kim, Do-Hyun Shin for your encouragement; Park's family (Mr. and Mrs. Park, Sungjin, Sunyoung, Jooyoung), Jee-Hoon Jeong, Yong-Sang Choi, Kukki Hong,

Seungjoo Park for your care and kindness; Se-Young, Yoon-Hwan, Soo-Hwan, Jenny Arvidsson, Michale Arvidsson for your love

My parents Sun-Yeon Choi and Chang-Gil Kang, my sister Mi-Seon and her husband Ji-Ho Bae for your endless love and encouragement

This project was supported by the research grants of the Biotechnology development project (2007-04306) from the Ministry of Education, Science and Technology of Korea, the VR Foundation, Hjalmar Svensson Research Foundation and Sylvans Foundation

8 References

[1] Branemark PI, Hansson BO, Adell R, Breine U, Lindstrom J, Hallen O, et al. Osseointegrated implants in the treatment of the edentulous jaw. Experience from a 10-year period. Scand J Plast Reconstr Surg Suppl. 1977;16:1-132.
[2] Albrektsson T, Wennerberg A. The impact of oral implants - past and future, 1966-2042. J Can Dent Assoc. 2005;71:327.
[3] Buser D, Thomas Nydegger Thomas Oxland David L. Cochran Robert K. Schenk Hans Peter Hirt Daniel Sn ivy Lutz-Peter Nolte. Interface shear strength of titanium implants with a sandblasted and acid-etched surface: A biomechanical study in the maxilla of miniature pigs. J Biomed Mater Res. 1999;45:75-83.
[4] De Groot K, Geesink R, Klein CP, Serekian P. Plasma sprayed coatings of hydroxylapatite. J Biomed Mater Res. 1987;21:1375-81.
[5] Ellingsen JE. Pre-treatment of titanium implants with fluoride improves their retention in bone. J Mater Sci Mater Med. 1995;6:749-53.
[6] Hall J, Lausmaa J. Properties of a new porous oxide surface on titanium implants. Applied Osseointegration Res. 2001;1:5-8.
[7] Ishizawa H, Fujino M, Ogino M. Mechanical and histological investigation of hydrothermally treated and untreated anodic titanium oxide films containing Ca and P. J Biomed Mater Res. 1995;29:1459-68.
[8] Kim HM, Miyaji F, Kokubo T, Nakamura T. Effect of heat treatment on apatite-forming ability of Ti metal induced by alkali treatment. J Mater Sci Mater Med. 1997;8:341-7.
[9] Sul YT. The significance of the surface properties of oxidized titanium to the bone response: special emphasis on potential biochemical bonding of oxidized titanium implant. Biomaterials. 2003;24:3893-907.
[10] Sul YT. Electrochemical growth behavior, surface properties, and enhanced in vivo bone response of TiO2 nanotubes on microstructured surfaces of blasted, screw-shaped titanium implants. Int J Nanomedicine. 2010;5:87-100.
[11] Sul YT, Byon ES, Jeong Y. Biomechanical measurements of calcium-incorporated oxidized implants in rabbit bone: effect of calcium surface chemistry of a novel implant. Clin Implant Dent Relat Res. 2004;6:101-10.
[12] Sul YT, Johansson C, Albrektsson T. Which surface properties enhance bone response to implants? Comparison of oxidized magnesium, TiUnite, and Osseotite implant surfaces. Int J Prosthodont. 2006;19:319-28.
[13] Wennerberg A, Ektessabi A, Albrektsson T, Johansson C, Andersson B. A 1-year follow-up of implants of differing surface roughness placed in rabbit bone. Int J Oral Maxillofac Implants. 1997;12:486-94.
[14] Wennerberg A, Albrektsson T, Johansson C, Andersson B. Experimental study of turned and grit-blasted screw-shaped implants with special emphasis on effects of blasting material and

surface topography. Biomaterials. 1996;17:15-22.
[15] Ellingsen JE, Johansson CB, Wennerberg A, Holmen A. Improved retention and bone-to-implant contact with fluoride-modified titanium implants. Int J Oral Maxillofac Implants. 2004;19:659-66.
[16] Mendes VC, Moineddin R, Davies JE. The effect of discrete calcium phosphate nanocrystals on bone-bonding to titanium surfaces. Biomaterials. 2007;28:4748-55.
[17] Buser D, Broggini N, Wieland M, Schenk RK, Denzer AJ, Cochran DL, et al. Enhanced bone apposition to a chemically modified SLA titanium surface. J Dent Res. 2004;83:529-33.
[18] Hanawa T, Kamiura Y, Yamamoto S, Kohgo T, Amemiya A, Ukai H, et al. Early bone formation around calcium-ion-implanted titanium inserted into rat tibia. J Biomed Mater Res. 1997;36:131-6.
[19] Gottlow J, Johansson C, Albrektsson T, Lundgren AK. Biomechanical and histologic evaluation of the TiUnite and Osseotite implant surfaces in rabbits after 6 weeks of healing. Appl Osseointegration Res. 2000;1:25-7.
[20] Lausmaa J. Surface spectroscopic characterization of titanium implant materials. J Electron Spectrosc. 1996;81:343-61.
[21] Sul YT, Johansson CB, Petronis S, Krozer A, Jeong Y, Wennerberg A, et al. Characteristics of the surface oxides on turned and electrochemically oxidized pure titanium implants up to dielectric breakdown: the oxide thickness, micropore configurations, surface roughness, crystal structure and chemical composition. Biomaterials. 2002;23:491-501.
[22] Keller EE, Tolman DE, Eckert S. Surgical-prosthodontic reconstruction of advanced maxillary bone compromise with autogenous onlay block bone grafts and osseointegrated endosseous implants: a 12-year study of 32 consecutive patients. Int J Oral Maxillofac Implants. 1999;14:197-209.
[23] Albrektsson T, Branemark PI, Hansson HA, Lindstrom J. Osseointegrated titanium implants. Requirements for ensuring a long-lasting, direct bone-to-implant anchorage in man. Acta Orthop Scand. 1981;52:155-70.
[24] Widmark G, Andersson B, Andrup B, Carlsson GE, Ivanoff CJ, Lindvall AM. Rehabilitation of patients with severely resorbed maxillae by means of implants with or without bone grafts. A 1-year follow-up study. Int J Oral Maxillofac Implants. 1998;13:474-82.
[25] Snauwaert K, Duyck J, van Steenberghe D, Quirynen M, Naert I. Time dependent failure rate and marginal bone loss of implant supported prostheses: a 15-year follow-up study. Clin Oral Investig. 2000;4:13-20.
[26] Friberg B, Grondahl K, Lekholm U, Branemark PI. Long-term follow-up of severely atrophic edentulous mandibles reconstructed with short Branemark implants. Clin Implant Dent Relat Res. 2000;2:184-9.
[27] Esposito M, Hirsch JM, Lekholm U, Thomsen P. Biological factors contributing to failures of osseointegrated oral implants. (I). Success criteria and epidemiology. Eur J Oral Sci. 1998;106:527-51.
[28] Nishiguchi S, Hirofumi Kato, Hiroshi Fujita, Hyun-Min Kim, Fumiaki Miyaji, Tadashi Kokubo, et al. Enhancement of bone-bonding strengths of titanium alloy implants by alkali and heat treatments. J Biomed Mater Res. 1999;48:689-96.
[29] Sul YT, Kang BS, Johansson C, Um HS, Park CJ, Albrektsson T. The roles of surface chemistry and topography in the strength and rate of osseointegration of titanium implants in bone. J Biomed Mater Res A. 2009;89:942-50.
[30] Yang GL, He FM, Song E, Hu JA, Wang XX, Zhao SF. In vivo comparison of bone

formation on titanium implant surfaces coated with biomimetically deposited calcium phosphate or electrochemically deposited hydroxyapatite. Int J Oral Maxillofac Implants. 2010;25:669-80.
[31] Sul YT, Johansson C, Albrektsson T. A novel in vivo method for quantifying the interfacial biochemical bond strength of bone implants. J R Soc Interface. 2010;7:81-90.
[32] Sul YT, Johansson C, Chang BS, Byon ES, Jeong Y. Bone tissue responses to Mg-incorporated oxidized implants and machine-turned implants in the rabbit femur. J Appl Biomater Biomech 2005;3:18-28.
[33] Sigel H. Metal ions in biological systems. Vol. 17, Calcium and its role in biology. New York: Marcel Dekker; 1984.
[34] Parsegian VA. Molecular forces governing tight contact between cellular surfaces and substrates. J Prosthet Dent. 1983;49:838-42.
[35] Collis JJ, Embery G. Adsorption of glycosaminoglycans to commercially pure titanium. Biomaterials. 1992;13:548-52.
[36] Hanawa T. In vivo metallic biomaterials and surface modification. Mat Sci Eng A-Struct. 1999;267:260-6.
[37] Gottlander M, Johansson CB, Albrektsson T. Short- and long-term animal studies with a plasma-sprayed calcium phosphate-coated implant. Clin Oral Implants Res. 1997;8:345-51.
[38] Albrektsson T. Hydroxyapatite-coated implants: a case against their use. J Oral Maxillofac Surg. 1998;56:1312-26.
[39] Sul YT, Johansson CB, Albrektsson T. Oxidized titanium screws coated with calcium ions and their performance in rabbit bone. Int J Oral Maxillofac Implants. 2002;17:625-34.
[40] Pham MT, Reuther H, Matz W, Mueller R, Steiner G, Oswald S, et al. Surface induced reactivity for titanium by ion implantation. J Mater Sci Mater Med. 2000;11:383-91.
[41] Endrino JL, Galindo RE, Zhang HS, Allen M, Gago R, Espinosa A, et al. Structure and properties of silver-containing a-C(H) films deposited by plasma immersion ion implantation. Surf Coat Technol. 2008;202:3675-82.
[42] Mendes VC, Moineddin R, Davies JE. Discrete calcium phosphate nanocrystalline deposition enhances osteoconduction on titanium-based implant surfaces. J Biomed Mater Res A. 2009;90:577-85.
[43] Sato M, Aslani A, Sambito MA, Kalkhoran NM, Slamovich EB, Webster TJ. Nanocrystalline hydroxyapatite/titania coatings on titanium improves osteoblast adhesion. J Biomed Mater Res A. 2008;84:265-72.
[44] Kang BS, Sul YT, Oh SJ, Lee HJ, Albrektsson T. XPS, AES and SEM analysis of recent dental implants. Acta Biomater. 2009;5:2222-9.
[45] Sul YT, Byon E, Wennerberg A. Surface characteristics of electrochemically oxidized implants and acid-etched implants: surface chemistry, morphology, pore configurations, oxide thickness, crystal structure, and roughness. Int J Oral Maxillofac Implants. 2008;23:631-40.
[46] Massaro C, Rotolo P, De Riccardis F, Milella E, Napoli A, Wieland M, et al. Comparative investigation of the surface properties of commercial titanium dental implants. Part I: chemical composition. J Mater Sci Mater Med. 2002;13:535-48.
[47] Coelho PG, Bonfante EA, Pessoa RS, Marin C, Granato R, Giro G, et al. Characterization of 5 Different Implant Surfaces and Their Effect on Osseointegration: A Study in Dogs. J Periodontol. 2010.
[48] Ohtsuka T, Nomura N. The dependence of the optical property of Ti anodic oxide film on its growth rate by ellipsometry. Corros Sci. 1997;39:1253-63.
[49] Hall J., Lausmaa J. Properties of a new porous oxide surface on titanium implants. Appl

Osseointegration Res. 2001;1:5-8.
[50] Fandridis J, Papadopoulos T. Surface characterization of three titanium dental implants. Implant Dent. 2008;17:91-9.
[51] Masaki C, Schneider GB, Zaharias R, Seabold D, Stanford C. Effects of implant surface microtopography on osteoblast gene expression Clin Oral Implants Res. 2005;16:650-6.
[52] Vidigal GM, Jr., Groisman M, de Sena LA, Soares Gde A. Surface characterization of dental implants coated with hydroxyapatite by plasma spray and biomimetic process. Implant Dent. 2009;18:353-61.
[53] Jarmar T, Palmquist A, Branemark R, Hermansson L, Engqvist H, Thomsen P. Characterization of the surface properties of commercially available dental implants using scanning electron microscopy, focused ion beam, and high-resolution transmission electron microscopy. Clin Implant Dent Relat Res. 2008;10:11-22.
[54] Fröjd V. On Ca^{2+} incorporation and nanoporosity of titanium surfaces and the effect on implant performance. Malmo: Malmo University; 2010.
[55] Hamlet S, Ivanovski S. Inflammatory cytokine response to titanium chemical composition and nanoscale calcium phosphate surface modification. Acta Biomater. 2011.
[56] Yang Y, Kim KH, Ong JL. A review on calcium phosphate coatings produced using a sputtering process--an alternative to plasma spraying. Biomaterials. 2005;26:327-37.
[57] Granato R, Marin C, Suzuki M, Gil JN, Janal MN, Coelho PG. Biomechanical and histomorphometric evaluation of a thin ion beam bioceramic deposition on plateau root form implants: an experimental study in dogs. J Biomed Mater Res B. 2009;90:396-403.
[58] Coelho PG, Lemons JE. Physico/chemical characterization and in vivo evaluation of nanothickness bioceramic depositions on alumina-blasted/acid-etched Ti-6Al-4V implant surfaces. J Biomed Mater Res A. 2009;90:351-61.
[59] Sul YT, Jönsson J, Yoon GS, Johansson C. Resonance frequency measurements in vivo and related surface properties of magnesium-incorporated, micropatterned and magnesium-incorporated TiUnite, Osseotite, SLA and TiOblast implants. Clin Oral Implants Res. 2009;20:1146-55.
[60] Coelho PG, Granato R, Marin C, Bonfante EA, Freire JNO, Janal MN, et al. Biomechanical Evaluation of Endosseous Implants at Early Implantation Times: A Study in Dogs. J Oral Maxil Surg. 2010;68:1667-75.
[61] Sul YT, Johansson C, Byon E, Albrektsson T. The bone response of oxidized bioactive and non-bioactive titanium implants. Biomaterials. 2005;26:6720-30.
[62] Zreiqat H, Valenzuela SM, Nissan BB, Roest R, Knabe C, Radlanski RJ, et al. The effect of surface chemistry modification of titanium alloy on signalling pathways in human osteoblasts. Biomaterials. 2005;26:7579-86.
[63] Anders A. Handbook of Plasma Immersion Ion Implantation and Deposition. Newyork: Wiely; 2000.
[64] Anders A. Metal plasma immersion ion implantation and deposition: a review. Surf Coat Technol. 1997;93:158-67.
[65] Brown IG. Cathod arc deposition of films. Annu Rev Mater Sci. 1998;28:243.
[66] Anders A, Anders S, Brown IG, Dickinson MR, MacGill RA, editors. Metal plasma immersion ion implantation and deposition using vacuum arc plasma sources. The first international workshop on plasma-based ion implantation; 1994; Madison, Wisconsin (USA): AVS.
[67] Anders A, Anders S, Brown IG, Yu KM. Increasing the retained dose by plasma

immersion ion-implantation and deposition. Santa Barbara, CA: Elsevier Science Bv; 1994:132-35.
[68] Anders A, Anders S, Brown IG, Yu KM. Increasing the retained dose by plasma immersion ion implantation and deposition. Nucl Instrum Meth B. 1995;102:132-5.
[69] Albrektsson T. Hydroxyapatite-coated implants: A case against their use. J Oral Maxillofac Surg. 1998;56:1312-26.
[70] Hench LL. Bioactive materials: The potential for tissue regeneration. J Biomed Mater Res. 1998;41:511-8.
[71] Sul YT. On the bone response to oxidized titanium implants: the role of microporous structure and chemical composition of the surface oxide in enhanced osseointegration. Gothenburg, Sweden, Department of Biomaterials/Handicap Research, University of Gothenburg; 2002.
[72] Sul YT, Johansson CB, Jeong Y, Albrektsson T. The electrochemical oxide growth behaviour on titanium in acid and alkaline electrolytes. Med Eng Phys. 2001;23:329-46.
[73] Park YJ, Shin KH, Song HJ. Effects of anodizing conditions on bond strength of anodically oxidized film to titanium substrate. Appl Surf Sci. 2007;253:6013-8.
[74] Hufner S. Photoelectron sepctroscopy: Principles and Applications. 3rd ed. Berlin Heidelberg, Germany: Springer-Verlag Berlin Heidelberg New York; 2003.
[75] Briggs D, Seah MP. Practical surface analysis. Chichester,Frankfurt: Wiley; 1990.
[76] Brundle CR, Evans CA, Wilson S, editors. Encyclopedia of materials characterization. Stoneham, USA: Butterworth-Heinemann & Manning publication; 1992.
[77] Moulder JF, Sobol PE, Stickle WF. Handbook of X-ray photoelectron spectroscopy : a reference book of standard spectra for identification and interpretation of XPS data. Eden Prairie, Minn.: Physical Electronics Inc.; 1995.
[78] Svanborg LM, Andersson M, Wennerberg A. Surface characterization of commercial oral implants on the nanometer level. J Biomed Mater Res B. 2010;92:462-9.
[79] Arvidsson A. On surface mediated interactions related to chemo-mechanical caries removal effects on surrounding tissues and materials. Gothenburg, Sweden, Department of Biomaterials/Handicap Research, University of Gothenburg; 2003.
[80] Wennerberg A, Albrektsson T. Suggested guidelines for the topographic evaluation of implant surfaces. Int J Oral Maxillofac Implants. 2000;15:331-44.
[81] Sul YT, Johansson C, Wennerberg A, Cho LR, Chang BS, Albrektsson T. Optimum surface properties of oxidized implants for reinforcement of osseointegration: surface chemistry, oxide thickness, porosity, roughness, and crystal structure. Int J Oral Maxillofac Implants. 2005;20:349-59.
[82] Sul YT, Jeong Y, Johansson C, Albrektsson T. Oxidized, bioactive implants are rapidly and strongly integrated in bone. Part 1 - experimental implants. Clin Oral Implants Res. 2006;17:521-6.
[83] Park JW, Kim YJ, Jang JH, Song H. Osteoblast response to magnesium ion-incorporated nanoporous titanium oxide surfaces. Clin Oral Implants Res. 2010;21:1278-87.
[84] Park JW, Park KB, Suh JY. Effects of calcium ion incorporation on bone healing of Ti6Al4V alloy implants in rabbit tibiae. Biomaterials. 2007;28:3306-13.
[85] Frojd V, Franke-Stenport V, Meirelles L, Wennerberg A. Increased bone contact to a calcium-incorporated oxidized commercially pure titanium implant: an in-vivo study in rabbits. Int J Oral Maxillofac Surg. 2008;37:561-6.
[86] Krupa D, Baszkiewicz J, Kozubowski JA, Barcz A, Sobczak JW, Biliniski A, et al. Effect

of calcium-ion implantation on the corrosion resistance and biocompatibility of titanium. Biomaterials. 2001;22:2139-51.
[87] Nayab SN, Jones FH, Olsen I. Effects of calcium ion implantation on human bone cell interaction with titanium. Biomaterials. 2005;26:4717-27.
[88] Omar OM, Lenneras ME, Suska F, Emanuelsson L, Hall JM, Palmquist A, et al. The correlation between gene expression of proinflammatory markers and bone formation during osseointegration with titanium implants. Biomaterials. 2011;32:374-86.
[89] Krupa D, Baszkiewicz J, Kozubowski JA, Barcz A, Sobczak JW, Bilinski A, et al. Effect of phosphorus-ion implantation on the corrosion resistance and biocompatibility of titanium. Biomaterials. 2002;23:3329-40.
[90] Lamolle SF, Monjo M, Lyngstadaas SP, Ellingsen JE, Haugen HJ. Titanium implant surface modification by cathodic reduction in hydrofluoric acid: surface characterization and in vivo performance. J Biomed Mater Res A. 2009;88:581-8.
[91] Lamolle SF, Monjo M, Rubert M, Haugen HJ, Lyngstadaas SP, Ellingsen JE. The effect of hydrofluoric acid treatment of titanium surface on nanostructural and chemical changes and the growth of MC3T3-E1 cells. Biomaterials. 2009;30:736-42.
[92] Ishizawa H. MFMO. Mechanical and histological investigation of hydrothermally treated and untreated anodic titanium oxide films containing Ca and P. J Biomed Mater Res. 1995;29:1459-68.
[93] Geesink RG, de Groot K, Klein CP. Bonding of bone to apatite-coated implants. J Bone Joint Surg Br. 1988;70:17-22.
[94] Ong JL, Bessho K, Cavin R, Carnes DL. Bone response to radio frequency sputtered calcium phosphate implants and titanium implants in vivo. J Biomed Mater Res. 2002;59:184-90.
[95] Siebers MC, Wolke JG, Walboomers XF, Leeuwenburgh SC, Jansen JA. In vivo evaluation of the trabecular bone behavior to porous electrostatic spray deposition-derived calcium phosphate coatings. Clin Oral Implants Res. 2007;18:354-61.
[96] Quaranta A, Iezzi G, Scarano A, Coelho PG, Vozza I, Marincola M, et al. A histomorphometric study of nanothickness and plasma-sprayed calcium-phosphorous-coated implant surfaces in rabbit bone. J Periodontol. 2010;81:556-61.
[97] Fini M, Cigada A, Rondelli G, Chiesa R, Giardino R, Giavaresi G, et al. In vitro and in vivo behaviour of Ca- and P-enriched anodized titanium. Biomaterials. 1999;20:1587-94.
[98] Pham MT, Reuther H, Matz W, Mueller R, Steiner G, Oswald S, et al. Surface induced reactivity for titanium by ion implantation. J Mater Sci Mater Med. 2000;11:383-91.
[99] Nishiguchi S, Nakamura T, Kobayashi M, Kim H-M, Miyaji F, Kokubo T. The effect of heat treatment on bone-bonding ability of alkali-treated titanium. Biomaterials. 1999;20:491-500.
[100] Fujibayashi S, Nakamura T, Nishiguchi S , Tamura J , Uchida M , Kim HM , et al. Bioactive titanium: Effect of sodium removal on the bone-bonding ability of bioactive titanium prepared by alkali and heat treatment. J Biomed Mater Res. 2001;56:562-70.
[101] Maitz MF, Poon RW, Liu XY, Pham MT, Chu PK. Bioactivity of titanium following sodium plasma immersion ion implantation and deposition. Biomaterials. 2005;26:5465-73.
[102] Baszkiewicz J, Krupa D, Kozubowski JA, Rajchel B, Lewandowska-Szumiel M, Barcz A, et al. The effect of sodium-ion implantation on the properties of titanium. J Mater Sci Mater Med. 2008;19:3081-91.
[103] Piotrowski O, Madore C, Landolt D. The mechanism of electropolishing of titanium in methanol-sulfuric acid electrolytes. J Electrochem Soc. 1998;145:2362-9.
[104] Anders A. Ion charge state distributions of vacuum arc plasmas: The origin of species.

Phys Rev E. 1997;55:969.
[105] Johansson C. On tissue reactions to metal implants. Gothenburg, Sweden, Department of Biomaterials/Handicap Research, University of Gothenburg; 1991.
[106] Rubo De Rezende ML, Johansson CB. Quantitative bone tissue response to commercially pure titanium implants. J Mater Sci Mater Med. 1993;4:233-9.
[107] Donath K, Breuner G. A method for the study of undecalcified bones and teeth with attached soft tissues. The Sage-Schliff (sawing and grinding) technique. J Oral Pathol. 1982;11:318-26.
[108] Frost HL. Presence of Microscopic cracks in vivo in bone. Henry Ford Hosp Med Bull. 1960;8:25-35.
[109] Kang BS, Sul YT, Jeong Y, Byon E, Kim JK, Cho S, et al. Metal plasma immersion ion implantation and deposition (MePIIID) on screw-shaped titanium implant: The effects of ion source, ion dose and acceleration voltage on surface chemistry and morphology. Med Eng Phys. 2011;33:730-38.
[110] Ivanoff CJ, Hallgren C, Widmark G, Sennerby L, Wennerberg A. Histologic evaluation of the bone integration of TiO(2) blasted and turned titanium microimplants in humans. Clin Oral Implants Res. 2001;12:128-34.
[111] Sul YT, Johansson CB, Kang Y, Jeon DG, Albrektsson T. Bone reactions to oxidized titanium implants with electrochemical anion sulphuric acid and phosphoric acid incorporation. Clin Implant Dent Relat Res. 2002;4:78-87.
[112] Yoshii S, Kakutani Y, Yamamuro T, Nakamura T, Kitsugi T, Oka M, et al. Strength of bonding between A-W glass-ceramic and the surface of bone cortex. J Biomed Mater Res. 1988;22:327-38.
[113] Schupbach P, Glauser R, Rocci A, Martignoni M, Sennerby L, Lundgren A, et al. The human bone-oxidized titanium implant interface: A light microscopic, scanning electron microscopic, back-scatter scanning electron microscopic, and energy-dispersive x-ray study of clinically retrieved dental implants. Clin Implant Dent Relat Res. 2005;7 Suppl 1:S36-43.
[114] Orsini G, Piattelli M, Scarano A, Petrone G, Kenealy J, Piattelli A, et al. Randomized, Controlled Histologic and Histomorphometric Evaluation of Implants With Nanometer-Scale Calcium Phosphate Added to the Dual Acid-Etched Surface in the Human Posterior Maxilla. J Periodontol. 2007;78:209-18.
[115] Browne M, Gregson PJ. Surface modification of titanium alloy implants. Biomaterials. 1994;15:894-8.
[116] Ronold HJ, Ellingsen JE. Effect of micro-roughness produced by TiO2 blasting--tensile testing of bone attachment by using coin-shaped implants. Biomaterials. 2002;23:4211-9.
[117] Shalabi MM, Gortemaker A, Hof MAVt, Jansen JA, Creugers NHJ. Implant Surface Roughness and Bone Healing: a Systematic Review. J Dent Res. 2006;85:496-500.